NAVAL POSTGRADUATE SCHOOL

MONTEREY, CALIFORNIA

THESIS

FOUR DIMENSIONAL ANALYSIS OF FREE ELECTRON LASERS IN THE AMPLIFIER CONFIGURATION

by

Juan R. Sans Aguilar

December 2007

Thesis Advisor: W. B. Colson
Second Reader: J. Blau

THIS PAGE INTENTIONALLY LEFT BLANK

REPORT DOCUMENTATION PAGE		Form Approved OMB No. 0704-0188

1. AGENCY USE ONLY *(Leave blank)*	2. REPORT DATE December 2007	3. REPORT TYPE AND DATES COVERED Master's Thesis

4. TITLE AND SUBTITLE Four Dimensional Analysis of Free Electron Lasers in the Amplifier Configuration	5. FUNDING NUMBERS
6. AUTHOR(S) J. R. Sans Aguilar	
7. PERFORMING ORGANIZATION NAME(S) AND ADDRESS(ES) Naval Postgraduate School Monterey, CA 93943-5000	8. PERFORMING ORGANIZATION REPORT NUMBER
9. SPONSORING /MONITORING AGENCY NAME(S) AND ADDRESS(ES) N/A	10. SPONSORING/MONITORING AGENCY REPORT NUMBER

11. SUPPLEMENTARY NOTES The views expressed in this thesis are those of the author and do not reflect the official policy or position of the Department of Defense or the U.S. Government.

12a. DISTRIBUTION / AVAILABILITY STATEMENT Approved for public release; distribution is unlimited.	12b. DISTRIBUTION CODE

13. ABSTRACT (maximum 200 words)

Free electron lasers (FEL's) are devices used worldwide for several purposes. In the military, especially in the Navy, they can be used for self-defense against missiles, and small boats. Installed on a ship, an FEL represents a multi-mission, deep magazine, long range weapon. This thesis will describe briefly the basic components and principles of operation. It also explores, by simulations, the effects of changing some of the parameters that generate the laser beam.

14. SUBJECT TERMS Free Electron Laser, FEL, Amplifier, High Energy Laser.	15. NUMBER OF PAGES 81
	16. PRICE CODE

17. SECURITY CLASSIFICATION OF REPORT	18. SECURITY CLASSIFICATION OF THIS PAGE	19. SECURITY CLASSIFICATION OF ABSTRACT	20. LIMITATION OF ABSTRACT
Unclassified	Unclassified	Unclassified	UU

NSN 7540-01-280-5500 Standard Form 298 (Rev. 2-89)
Prescribed by ANSI Std. 239-18

THIS PAGE INTENTIONALLY LEFT BLANK

Approved for public release; distribution is unlimited

FOUR DIMENSIONAL ANALYSIS OF FREE ELECTRON LASERS IN THE AMPLIFIER CONFIGURATION

Juan R. Sans Aguilar
Lieutenant, Mexican Navy
S.W.O., Mexican Naval Academy, 1994

Submitted in partial fulfillment of the
requirements for the degree of

MASTER OF SCIENCE IN APPLIED PHYSICS

from the

NAVAL POSTGRADUATE SCHOOL
December 2007

Author: Juan R. Sans Aguilar

Approved by: William B. Colson
Thesis Advisor

Joseph Blau
Second Reader

James Luscombe
Chairman, Department of Physics

THIS PAGE INTENTIONALLY LEFT BLANK

ABSTRACT

Free electron lasers (FEL's) are devices used worldwide for several purposes. In the military, especially in the Navy, they can be used for self-defense against missiles, and small boats. Installed on a ship, an FEL represents a multi-mission, deep magazine, long range weapon. This thesis will describe briefly the basic components and principles of operation. It also explores, by simulations, the effects of changing some of the parameters that generate the laser beam.

THIS PAGE INTENTIONALLY LEFT BLANK

TABLE OF CONTENTS

THIS PAGE INTENTIONALLY LEFT BLANK

LIST OF FIGURES

LIST OF TABLES

THIS PAGE INTENTIONALLY LEFT BLANK

ACKNOWLEDGMENTS

I’d like to thank Professors Bill Colson, Joe Blau and Robert Armstead for their aid in the preparation of this work, without them this work would not be possible.

Special thanks to my wife, Rosa, for her understanding and help during the time I spent in this work.

THIS PAGE INTENTIONALLY LEFT BLANK

I. INTRODUCTION

A. HISTORY OF THE LASER

The word “laser” is an acronym for “light amplification by the stimulated emission of radiation”. Laser is an optical source that emits nearly monochromatic light in a narrow coherent beam.

The laser was proposed as a variation of the maser (“Microwave amplification by the stimulated emission of radiation”) principle in the late 1950s and was demonstrated in July 1960 by Theodore Maiman at Hughes research laboratories [1].

Albert Einstein, in his 1916 paper, ***Strahlungs-Emission und-absorption nach der Quantentheorie,*** laid the foundation of the laser and the maser. He applied Max Planck’s law of radiation in terms of the probability of absorption and spontaneous and stimulated emission. In 1928, Rudolph W. Landenburg confirmed the existence of stimulated emission and negative absorption experimentally. In 1939, the Russian, Valentin A. Fabrikant, suggested the use of stimulated emission to amplify “Short” waves. In 1947, Willis E. Lamb and R.C. Retherford demonstrated apparent stimulated emission in hydrogen spectra. Finally in 1950 Alfred Kastler proposed the method of optical pumping, which was experimentally confirmed by Brossel, Kastler and Winter two years later [1].

In 1953, Charles H Townes, James P Gordon and Herbert J. Zeiger made the first “Maser” to produce microwave radiation. In 1957, Townes and Arthur L. Schawlow began to produce emissions in the infrared band and then adapted it

to optical wavelengths. In 1958, Prokhorov proposed the usage of an open resonator in the maser, and Schawlow and Townes settled on an open resonator design[1].

The first working laser was made by Theodore Maiman in 1960 in Malibu, California; a collaboration of several institutions. This laser was made with a synthetic ruby crystal, pumped by a flashlamp to produce light at wavelength 694 nm [1].

In 1960, Ali Javan, William Bennet and Donald Heriot made the first gas laser using Helium and Neon [1].

The first ***laser diode*** was made by Robert N. Hall in 1962. It was made of gallium arsenide and emitted in the near-infrared at 850 nm. The first semiconductor laser with visible emission was made the same year by Nick Holonyak, Jr. These semiconductor lasers could be used only in pulsed operation, and indeed only when cooled to liquid nitrogen temperatures (77 K) [1].

In 1970, Zhores Alferov in the Soviet Union and Izuo Hayashi and Morton Panish of Bell Telephone Laboratories independently developed laser diodes continuously operating at room temperature, using the heterojunction structure [1].

B. HISTORY OF A FREE ELECTRON LASER

The Free Electron Laser (FEL) appeared in the middle 1970s, with the well-documented experiments at Stanford by Dr. John M.J. Madey (professor at that university until 1988). The FEL by itself has a background which dates back to at least 1947 and a patent by Elmer Gorn, in which he describes amplification producing fast electromagnetic wave (periodic electron beam) interactions [2].

In the 1950s, Motz worked on an undulator, and he passed a beam from a 3-MeV accelerator through it to produce millimeter wave radiation. He later used a 100-MeV beam to produce visible light. Another experiment of Motz was the Ubitron, a mildly relativistic microwave FEL. The power capability of this device was so much greater than that of conventional klystrons and magnetrons that records for peak power generation, which would stand for two decades, were established at both centimeter and millimeter wavelengths [2].

Nowadays the tendency of the institutions is to design FELS to operate at shorter wavelengths. The most powerful FEL in the United States is located in Jefferson's Lab at Newport News, Virginia; having a power of 14 kilowatts, this device works in an oscillator configuration.

C. ADVANTAGES AND DISADVANTAGES OF THE FREE ELECTRON LASER

The Free Electron laser has several advantages over other lasers. It is more flexible than the others; for example, it is tunable by design. That means that the output wavelength can be changed as desired by changing the energy of the electron beam or the properties of the undulator. A second advantage is that the FEL can operate continuously (24 hours a day) at a relatively low cost, whereas chemical lasers have to be replenished after a short time of operation, and they may generate toxic exhausts. The FEL will operate all the time if it has a continuous power supply and will not damage the environment with a toxic exhaust. Also, FEL can reach higher powers than the chemical lasers, because their lasing medium does not get hot.

THIS PAGE INTENTIONALLY LEFT BLANK

II. BASIC COMPONENTS OF A FREE ELECTRON LASER

There are two basic configurations of a free electron laser: The oscillator configuration and the amplifier configuration. Both configurations have many common components; the difference is in the way that the laser beam is generated. The basic components are: injector, linear accelerator, undulator, resonator (or, for the amplifier, a laser seed), beam dump and accessories. Figure 1 shows the basic components of a free electron laser.

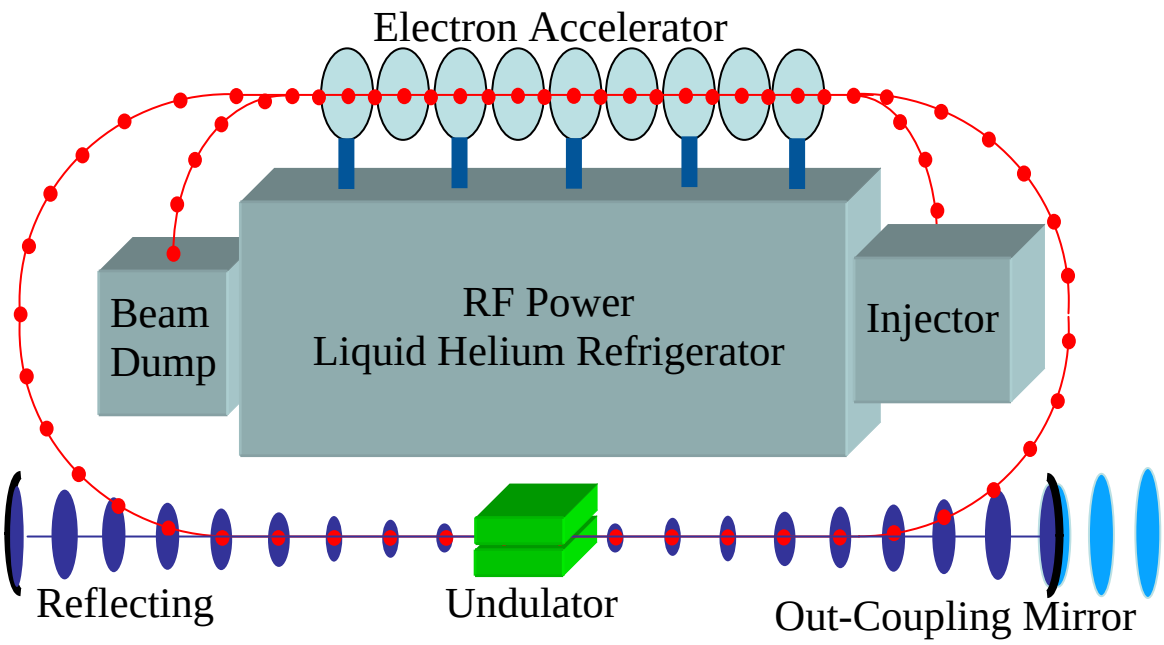

Figure 1. Basic components of a free electron laser (oscillator mode) from [3].

A. THE INJECTOR

This is the first part of the device and is the source of the electron beam. Basically it contains a cathode, as does a TV tube. The electron beam is generated in short pulses (on the order of picoseconds) with energy of 5 MeV approximately, a value common to both configurations. There are several types of injectors; among these we can find the direct-current injector (DC), the radio-frequency injector (RF) and the semiconducting radio-frequency injector; and all of them can be used in an FEL system. Some injectors are driven by a laser in order to provide the required beam; the drive laser consists of a diode-pumped Nd:Glass oscillator and a chirped pulse amplification system consisting of a granting stretcher, a flashlamp-pumped Nd:Glass regenerative amplifier and a grating compressor [8]. Figure 2 shows a basic scheme of a photocathode injector.

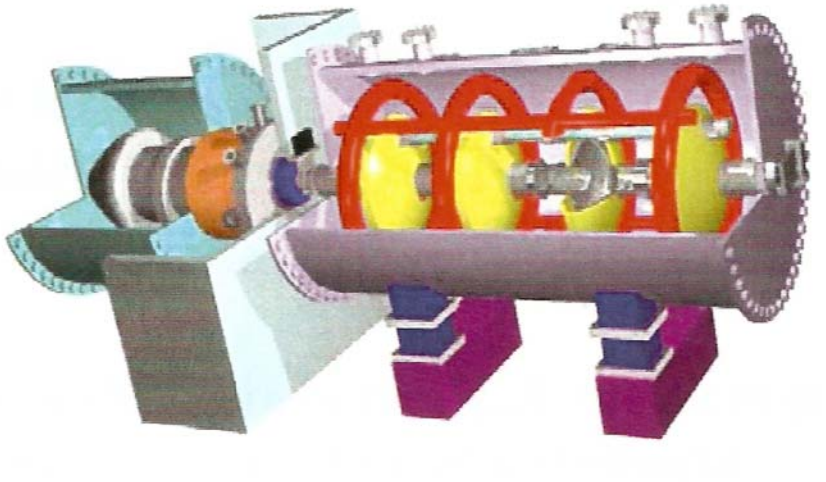

Figure 2. Basic scheme of a photocathode injector from [4].

B. LINEAR ACCELERATOR

The linear accelerator (linac) is a critical component of the equipment, and increases the energy of the electron beam from 5 MeV at the output of the injector to about 100 MeV. This increment of energy is done in the accelerator RF cavities. Electrons gain energy from the RF fields as they go from one cavity to the next, traveling through an electric field. The efficiency and gradient of the linac, and therefore the entire system, can be increased by use of a superconducting accelerator, which must operate at cryogenic temperatures. This requires the installation of a liquid helium refrigerator. Figure 3 shows the schematic of a linear accelerator.

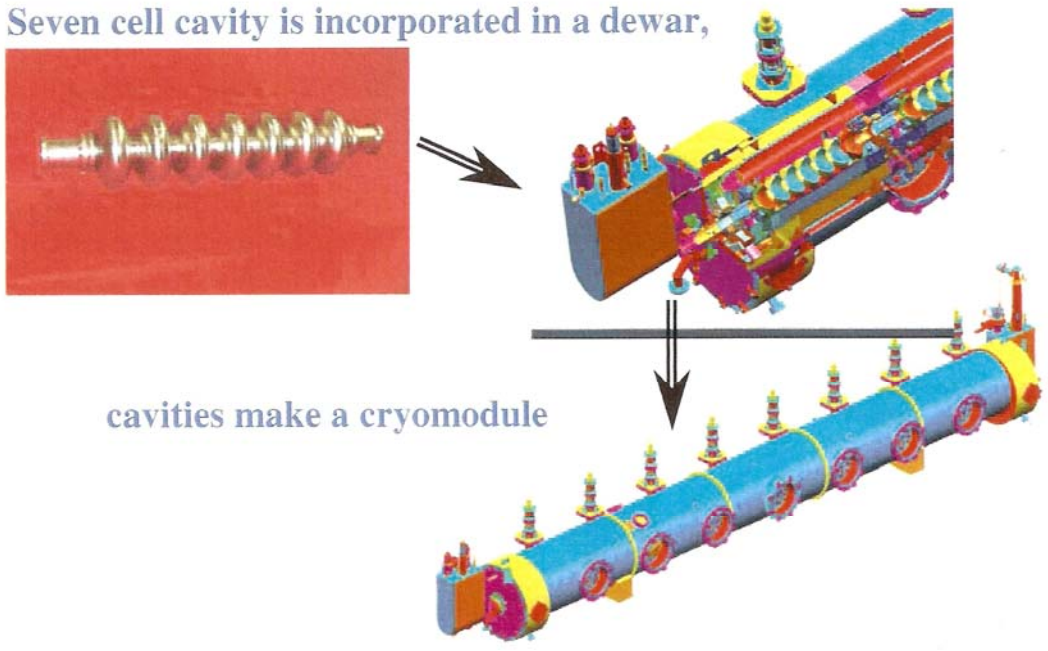

Figure 3. Schematic of a linear accelerator from [4].

C. UNDULATOR

The undulator is where the laser beam is created and enhanced, and where much of the interesting physics occur. An undulator is a series of alternating magnets, typically forming about 20 – 100 periods, separated by a few centimeters, and delivering a typical magnetic peak field of about 1 Tesla. The characteristics of the laser beam are determined by the undulator design, being a region in which the electrons are made to wiggle by a static alternating magnetic field. Since wiggling electrons radiate light, we can store this light in a resonator; and we can stimulate emission by radiating in the presence of this same light. While electrons are in the presence of the light there is an exchange of energy to and from the light. The electron distribution in phase space must be arranged in order to obtain the most efficient transfer of energy from the electrons to the light. Additional information will be written about this effect in a later chapter. In the amplifier configuration, the light passes only one time through the undulator, and then we require a longer undulator to extract the largest possible energy from the electron beam. Figure 4 shows the basic architecture of an undulator.

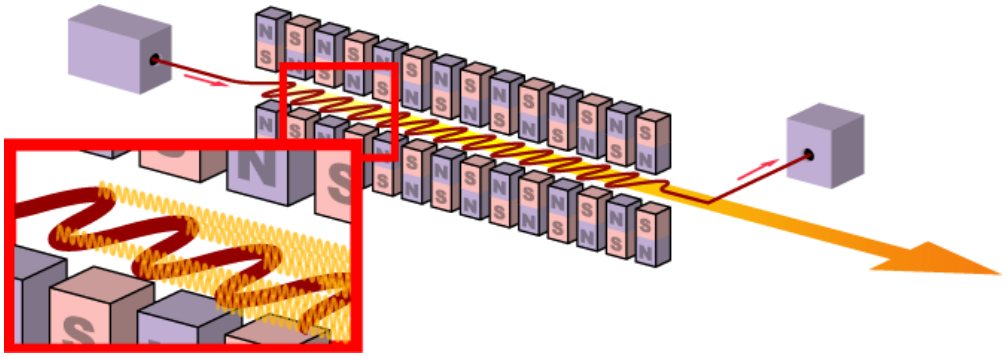

Figure 4. Schematic of an undulator from [6].

D. RESONATOR

The resonator is the component where the light is stored in the oscillator configuration. It consists of an evacuated cavity bracketed by two mirrors typically separated by 20 – 30 meters, between which the light is stored. One of the mirrors is perfectly reflective (100%), the other is partially transmitting (it transmits some percentage of the light). It is through this mirror that the laser beam escapes to the outside. Resonators are often characterized by their quality factor Q, which is established by the inverse of their loss per pass (1 / Loss per pass). Figure 5 shows a basic arrangement of a resonator.

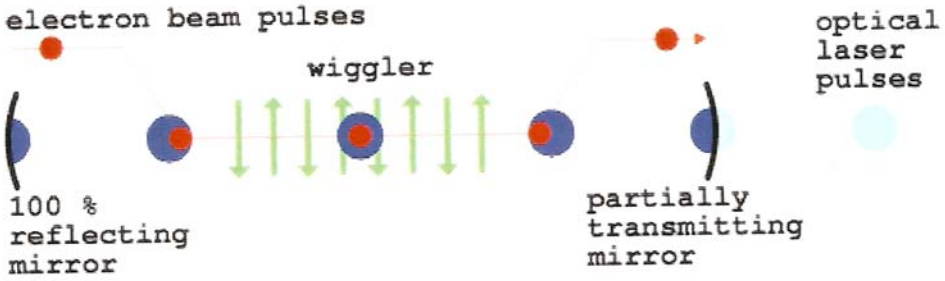

Figure 5. Schematic of a resonator from [3].

E. SEED LASER

For an amplifier configuration it is necessary to have an external laser source, because unlike the oscillator, no light is stored in the optical cavity. This external laser source is the "seed laser"; it generates a laser beam of weak field (low power usually 10 – 100 W) that is introduced to the undulator for amplification to the desired output (1 MW in our case). Figure 6 shows a basic arrangement of a seed laser.

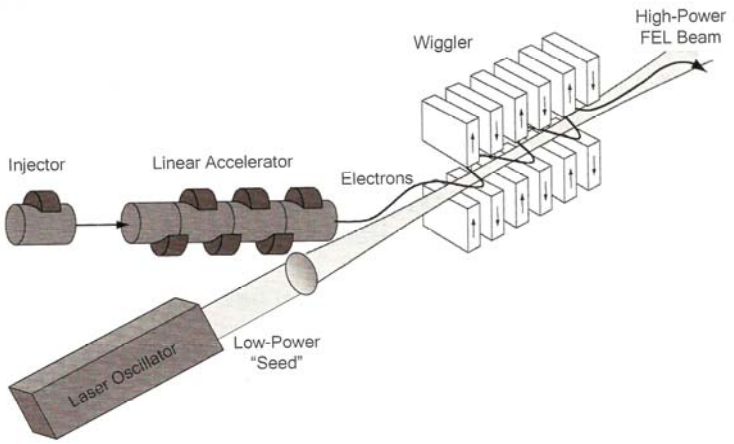

Figure 6. Arrangement of a seed laser from [5].

F. ACCESSORIES

"Accessories" implies all the devices that control the behavior of the beams (electron and optical). They consist of bending and focusing magnets that center the electron beam and change its direction, and the mirrors that direct the optical beam.

G. ELECTRON BEAM DUMP

It is the last part of the electron path. In an FEL with recirculation of the electron beam, the electrons enter to the linac a second time 180° out of phase with the RF fields, giving most of their energy back to the electric field. At the output of the linac, the recirculated electron beam has energy of about 5 MeV, which is about the same energy that they have when they are generated at the injector. These electrons, with the residual energy, are dumped into what is called the "electron beam dump." At that relatively low energy, the electrons create less heat and radiation, so less shielding is required on this electron beam dump.

III. BASIC THEORY OF A FREE ELECTRON LASER

A. THE PENDULUM EQUATION

Since an accelerated charged particle emits radiation, we can create radiation by accelerating electrons inside the undulator. We do this by making the relativistic electrons 'wiggle' through the undulator. When an electron enters to the undulator, it goes through electric and magnetic fields and encounters a force that acts upon it given by the Lorentz force equation. For relativistic electrons in the undulator, the complete Lorentz FEL force equations are given by [3]

$$\frac{d\left(\gamma\vec{\beta}\right)}{dt} = -\frac{e}{mc}\left(\vec{E} + \vec{\beta} X \vec{B}\right), \qquad \text{(III.1)}$$

$$\frac{d\gamma}{dt} = -\frac{e}{mc}\vec{\beta} X \vec{E}, \qquad \text{(III.2)}$$

$$\frac{1}{\gamma^2} = 1 - \vec{\beta}^2, \qquad \text{(III.3)}$$

where e is the electron charge magnitude, m the electron mass, $\vec{E}$ the electric field, $\vec{B}$ the magnetic field, $\vec{\beta} = \vec{\nu}/c$, $\vec{\nu}$ is the electron velocity, c is the speed of light and γ is the relativistic Lorentz factor.

If we substitute the electric and magnetic fields of the FEL into equation (III.1), we get

$$\frac{d\left(\gamma\vec{\beta_\perp}\right)}{dt} = -\frac{e}{mc}\left[E\left(1-\beta_z\right)\left(\cos\psi, -\sin\psi, 0\right) + \beta_z B\left(-\sin\left(k_o z\right), \cos\left(k_o z\right), 0\right)\right] \qquad \text{(III.4)}$$

$$\frac{d\left(\gamma\vec{\beta_z}\right)}{dt} = -\frac{e}{mc}\left[E\left(\beta_x\cos\psi - \beta_y\sin\psi\right) + B\left(\beta_x\sin\left(k_o z\right) - \beta_y\cos\left(k_o z\right)\right)\right] \qquad \text{(III.5)}$$

where $\beta_z = \sqrt{1-\left(1/\gamma^2\right)\left(K^2+1\right)}$ is the magnitude of the longitudinal *z* component of the electron velocity, E is the magnitude of the electric field, B is the magnitude of the magnetic field and ψ is the phase. We can solve for the transverse velocity components $\vec{\beta}_\perp = -\left(K/\gamma\right)\left(\cos\left(k_o z\right), \sin\left(k_o z\right), 0\right)$ where β_x and β_y are the components of the velocity and $K = eB\lambda_o / 2\pi mc^2$.

Substituting the transverse velocity components $\vec{\beta}_\perp$ into (III.2) we get

$$\overset{\circ}{\gamma} = -\frac{e}{mc}\vec{\beta}\cdot\vec{E} = \frac{cKE}{\gamma mc}\left(\cos k_o z \cos\psi - \sin k_o z \sin\psi\right) = \frac{cKE}{\gamma mc}\cos\left(\zeta+\phi\right), \qquad \text{(III.6)}$$

where $\zeta \equiv \left(k_0 + k\right)z - \omega t$ is the electron phase, which represents the position of the electron within an optical wavelength. If we take the derivative of the electron phase with respect to the dimensionless time $\tau = ct/L$, where $L = N\lambda_o$ is the length of the undulator, and *N* the number of periods of the undulator, we get the electron phase velocity

$$\nu = \overset{\circ}{\zeta} = L\left[\left(k+k_o\right)\beta_z - k\right].$$

For highly relativistic electrons $\left(\gamma >> 1\right)$, we can approximate $\beta_z \approx 1-\left(K^2+1\right)/2\gamma^2$, and near resonance $\left(k >> k_o\right)$, so that the derivative of the electron phase becomes

$$\overset{\circ}{\zeta} = L\left[\left(k+k_o\right)\left(1-\left(K^2+1\right)/2\gamma^2\right)-k\right] = Lk\left(1-\left(K^2+1\right)/2\gamma^2\right).$$

If we take the second derivative of the electron phase, we get

$$\overset{\circ\circ}{\zeta} = \frac{\overset{\circ}{\gamma} L^2 k}{c}\left(1-\left(K^2+1\right)/\gamma^3\right).$$

Substituting (III.6) into the last equation and defining $|a| = 4\pi NeK|E|L/\gamma^2 mc^2$ as the dimensionless field amplitude, we obtain the dimensionless pendulum equation,

$$\ddot{\zeta} = \dot{\nu} = |a|\cos(\zeta + \phi)\,. \qquad \text{(III.7)}$$

This equation describes the microscopic motion of electrons in phase space within the undulator.

B. PHASE SPACE

The phase space representation is a diagram that shows the evolution in position and velocity coordinates. It is useful to show, as in the last section, the electron energy exchange in an FEL. This diagram shows the electron phase velocity versus the phase. There are two types of orbits on a phase space diagram: closed and open orbits.

Closed orbits for a classical pendulum represent a pendulum swinging back and forth; open orbits occur when the pendulum goes over the top due to a large angular velocity. The border between those two states is called the separatrix. Figure 7 shows a separatrix (black line) and the closed (green line) and open (red doted line) orbits on a phase space diagram; horizontal axis is the angular displacement and vertical axis the angular velocity.

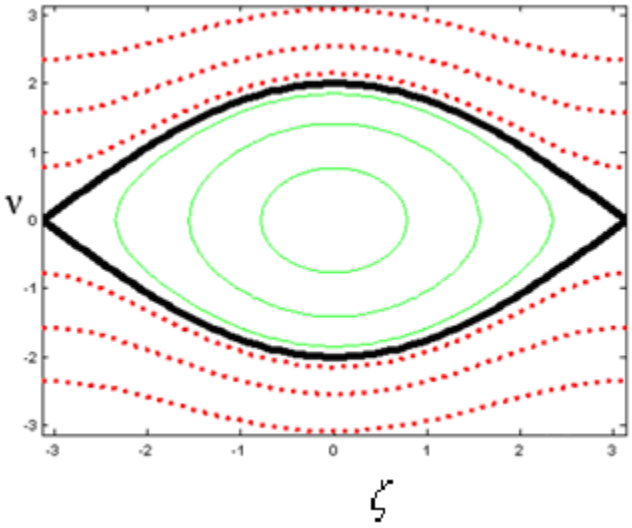

Figure 7. Separatrix and orbits on a pendulum phase space diagram.

Since we suggested the similarity between the FEL and a pendulum, and we obtained a pendulum equation describing the behavior of electrons in an FEL, we can state that $|a|$ and ϕ are roughly constant for the case of low gain in the FEL; in the same way, the electron phase ζ can be viewed as the electron's position within an optical wavelength, and ν is its phase velocity relative to resonance (ν=0).

For the FEL, the separatrix is given by [3]:

$$\nu^2 = 2|a|\left[1+\sin\left(\zeta+\phi\right)\right] \qquad \text{(III.8)}$$

Figure 8 shows a phase space diagram of the behavior of approximately 20 electrons evenly spaced in ζ with ν_o=0 in a free electron laser. Yellow color indicates the electrons at the beginning of the undulator (τ=0) and blue color indicates the electrons at the end of the undulator (τ=1). In this particular situation the gain of the system is zero, because half of the electrons gain energy and half of the

electrons lose it. In order to get gain, it is necessary to initiate the process with the electrons off resonance as Figure 9 shows.

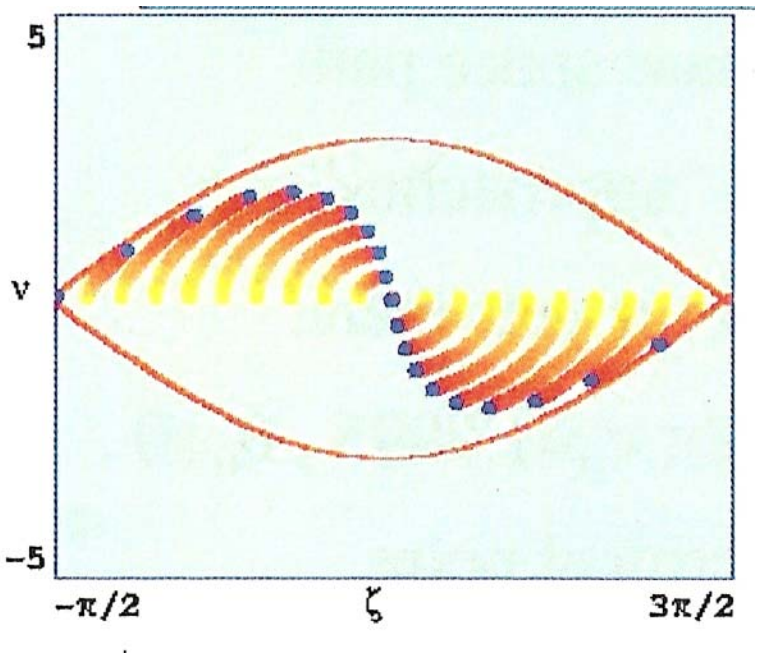

Figure 8. FEL phase space diagram from [3]

C. ELECTRON BEAM AND OPTICAL BEAM INTERACTION

One important issue in an FEL is the energy exchange between electrons and the optical field. As noted previously, values of ν close to resonance (ν=0) are required for optimal energy exchange. Phase space evolutions of the electrons showing a good bunching or grouping result in bigger gain. So it is necessary to create an optimal bunching to get the best values of gain.

Figure 9 shows a phase space diagram of the evolution of the electrons in a free electron laser for a more realistic beam with 1000 particles and a small initial energy spread.

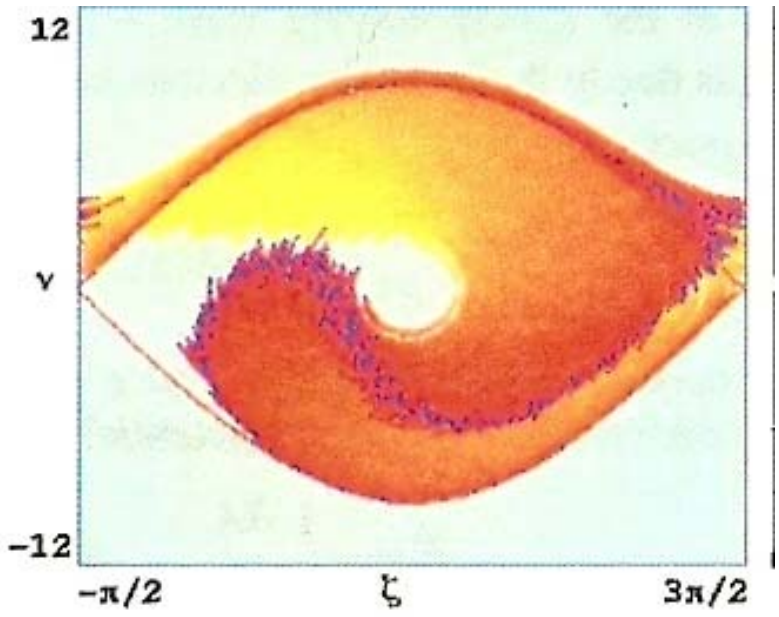

Figure 9. FEL electron's bunching from [3].

D. FEL WAVE EQUATION

From Maxwell's equations, we can obtain a full wave equation for the FEL optical field in terms of the transverse current [3]:

$$\nabla^2\mathbf{A}-\frac{1}{c^2}\frac{\partial^2\mathbf{A}}{\partial t^2}=-\frac{4\pi}{c}\mathbf{J}_\perp \quad , \qquad \text{(III.9)}$$

where **A** is the optical magnetic vector potential and **J** is the current density.

For our helical undulator, a form for the optical vector potential can be written as [3]:

$$\mathbf{A}(\mathbf{x},t)=\frac{\mathbf{E}(\mathbf{z},t)}{k}\hat{\varepsilon}e^{\mathbf{i}\alpha} \quad , \qquad \text{(III.10)}$$

where **E**(**z**,t) is the complex optical amplitude, $\alpha = kz-\omega t$ is the carrier wave phase, $\mathbf{i}=(-i,1,0)$ is the optical field's

polarization vector for circularly polarized light, and $\mathbf{x} = x\hat{\mathbf{i}} + y\hat{\mathbf{j}} + z\hat{\mathbf{k}}$ is the position vector.

Substituting the solution in the wave equation we can get the results for the four dimensions. We can make some simplifications and substitutions like the slowly varying amplitude and phase approximation that will be discussed later in this chapter, in order to get the FEL wave equation as [3]:

$$\frac{\partial a(\tau)}{\partial \tau} = < -je^{-i\zeta} > \quad , \qquad \text{(III.11)}$$

where $a(\tau) = |a|e^{i\phi}$ is the complex dimensionless optical field amplitude; the dimensionless current is $j = 8N(e\pi KL)^2 n_e / \gamma^3 mc^2$, where n_e is the beam particle density, measuring the interaction between the electron beam and the optical mode; and $< e^{-i\zeta} >$ measures the amount of electron bunching. If j is large ($j >> \pi$), the optical field a changes rapidly, so we have high gain. If j is small ($j \leq \pi$), we have low gain.

E. WEAK FIELD GAIN

As mentioned previously, we can obtain gain through the interaction of the bunched electron beam with the optical field inside the undulator. An optical field is considered weak when $|a| < \pi$ it is smaller than π. The following wave equations are valid for weak and strong optical fields [3]:

$$\frac{d|a|}{d\tau} = -j\left\langle \cos(\zeta + \phi) \right\rangle, \text{ and} \qquad \text{(III.12)}$$

$$\dot{\phi} = \frac{j}{|a|}\left\langle \sin(\zeta + \phi) \right\rangle . \qquad \text{(III.13)}$$

They describe the change in optical amplitude $|a|$ and phase φ during FEL interaction with the electron beam. The pointing brackets denote the average of all the electrons sampled within an optical wavelength of the beam.

From the coupling between the electron beam and optical field, we can calculate the dimensionless current density j.

1. Low Gain Regime (j ≤ π)

In this regime, since j is small there is not an appreciable change in the optical field amplitude or phase as the electrons pass through the undulator. The evolution of the optical field amplitude and phase versus τ (dimensionless time for the electrons to pass through the undulator from τ=0 through τ=1) can be obtained by expanding ζ and ν in powers of $|a| = a_0$ to get [7]

$$|a(\tau)| = a_0\left[1 + j\left(\frac{2-2\cos(\nu_0\tau)-\nu_0\tau\sin(\nu_0\tau)}{2\nu_0^3}\right)\right] \qquad \text{(III.14)}$$

$$\phi(\tau) = j\left(\frac{2\sin(\nu_0\tau)-\nu_0\tau(1+\cos(\nu_0\tau))}{2\nu_0^3}\right) \qquad \text{(III.15)}$$

where a_0 is the initial optical field amplitude, and ν_0 is the initial phase velocity of the electron beam.

In an FEL system, the gain is sensitive to the initial phase velocity ν_0. If the electron beam starts with $\nu_0 = 0$ (at resonance), the resultant gain is negligible. The resulting gain inside the undulator assuming weak fields is given by [7]

$$G(\tau) = j\left(\frac{2-2\cos(\nu_0\tau)-\nu_0\tau\sin(\nu_0\tau)}{\nu_0^3}\right) \qquad \text{(III.16)}$$

2. High Gain Regime (j>>π)

In this regime, the dimensionless current density is large, and it strongly affects the optical field amplitude and phase as the electrons go through the undulator. In this case, the optical field amplitude and phase during the electron beam interaction with the optical field are given by [7]

$$\left|a(\tau)\right| = \frac{a_0}{3} e^{\left(\frac{j}{2}\right)^{\frac{1}{3}} \frac{\sqrt{3}\tau}{2}} \quad \text{, and} \qquad \text{(III.17)}$$

$$\phi(\tau) = \left(\frac{j}{2}\right)^{1/3} \frac{\tau}{2} \quad . \qquad \text{(III.18)}$$

From these formulas, we can see large changes in the amplitude and phase due to the current density; then for large changes in the phase, the separatrix is shifted and the optimum bunching location changes on the phase space diagram. In contrast to the low gain regime, the gain is not as sensitive to the initial phase velocity, but the gain spectrum changes as well.

The expression for the gain in the undulator for this regime is given by [7]

$$G(\tau) = \frac{1}{9} e^{\left(\frac{j}{2}\right)^{\frac{1}{3}} \frac{\sqrt{3}\tau}{2}} \quad . \qquad \text{(III.19)}$$

F. STRONG FIELD GAIN

For this case, in both regimes (low and high gain), strong optical fields make the electron beam overbunch in the undulator as the electrons travel in it. This process is called saturation. Overbunching creates absorption of energy by the electrons from the optical field, reducing the gain of the system. In the low gain regime, saturation is

achieved at much lower initial field amplitudes $(a_s \approx \pi)$ than the high gain regime $a_s \approx 2(j/2)^{2/3}$ [7].

When there is not saturation, the phase space evolution of the electrons is slower and the bunch of electrons travel downward to a phase of ζ ≈ π. However, the stronger optical field causes a greater force on the electrons and more evolution in phase space. The bunch forms and continues along closed orbits until it begins an upward trend, taking the energy away from the optical field.

G. TAPERED WIGGLER

In this work, an analysis of an FEL in the amplifier configuration is made; this type of system requires a much longer undulator than the oscillator. If we want to increase the gain and extraction of the system, we can extend the saturation of electrons by tapering the undulator. Taper is a change in the resonance condition $\lambda = \frac{\lambda_o}{2\gamma^2}\left(1+K^2\right)$ as the electrons travel along the undulator; this alteration extends the energy exchange between electrons and the optical field; this extended exchange allows a greater amount of energy taken from the electrons and an increased extraction of energy from the device. As the electrons evolve, they loose energy, and γ decreases, then, in order to keep the same wavelength, λ_o or K must be decreased.

There are several ways to taper the undulator; the most common is to vary the undulator parameter K by changing the magnetic fields along it. The easiest way to do this taper is to change the size of the gap between magnets by a small amount (Tenths of millimeters); this will change the

strength of the field at certain points. In this way, we can generate different types of tapering.

1. Linear Tapering

This tapering method consists of a continuous increment or decrement of the magnetic field strength along the undulator. This variation of the field can be negative (increasing gap) or positive (decreasing gap). The taper can start at any location along the undulator and continues linearly through the rest of the undulator. Typically, the taper stars near the location where the optical field is expected to reach its saturation value a_s.

As we can see in Figures 10 and 11 (positive and negative linear taper), this technique exposes the electron beam to a linearly changing magnetic field.

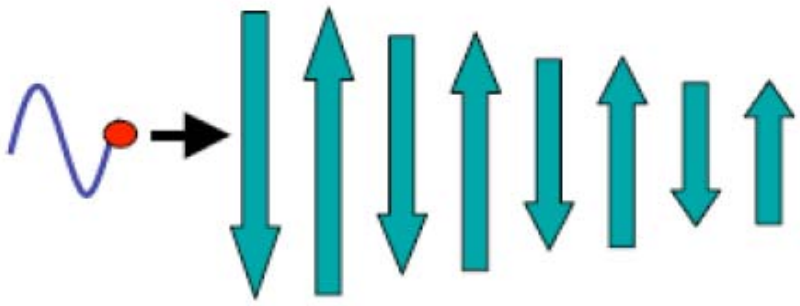

Figure 10. Positive linear tapered undulator from [3].

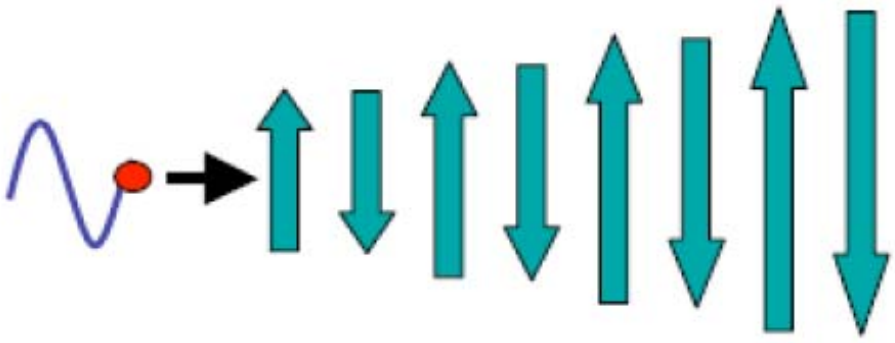

Figure 11. Negative linear tapered undulator from [3].

2. Step-Tapering

Other useful taper method is the step taper. This method consists of changing the gap at a certain point within the undulator and maintaining this gap through the rest of it. Figures 12 and 13 show a positive and a negative step-tapered undulator.

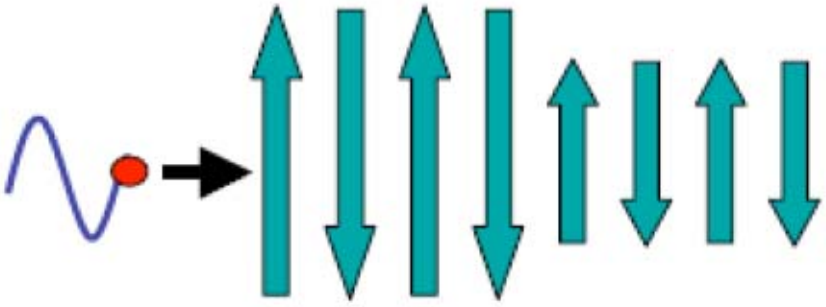

Figure 12. Positive step-tapered undulator from [3].

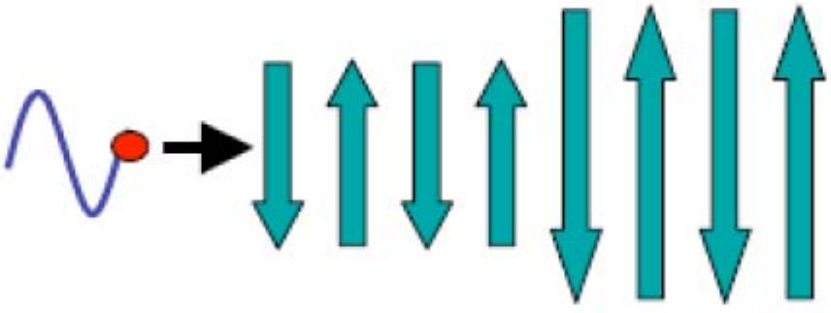

Figure 13. Negative step-tapered undulator from [3].

As the electron beam's energy changes along the undulator, the resonance condition is altered. By tapering the undulator, we introduce the following phase acceleration in the pendulum equation [7]:

$$\delta = -4\pi N \frac{K^2}{1+K^2}\frac{\Delta K}{K} \qquad \text{(III.20)}$$

where ΔK/K is the fractional change on the undulator parameter, and where K is proportional to the magnetic field.

The pendulum equation for the tapered undulator becomes [7]:

$$\overset{\circ\circ}{\zeta} = \overset{\circ}{\nu} = \delta + |a|\cos(\zeta + \phi) \quad . \qquad \text{(III.21)}$$

The optimal extraction from a normal undulator is [7]:

$$\eta \approx \frac{1}{2N} \quad , \qquad \text{(III.22)}$$

but in a tapered undulator, the phase acceleration δ plays an important role in the extraction. The extraction for this case is [7]:

$$\eta_\delta \approx \frac{|\delta|}{8\pi N} \quad . \qquad \text{(III.23)}$$

As the phase acceleration (positive or negative) approaches the value of the optical field amplitude, the separatrix becomes smaller. When this acceleration is greater, the separatrix vanishes, and bunching does not occur because the electrons are not trapped.

It is obvious that at bigger phase acceleration, the extraction will be bigger; but there is an upper limit. This limit is set by the fact that the pendulum equation has no solution when the taper phase acceleration is bigger than the optical field amplitude; however, a lower limit is

determined by the maximum deceleration a tapered electron can undergo in the no tapered case. Then, we can state the taper range as:

$$4\sqrt{a} < \delta < |a|$$

Figures 14 and 15 show the phase space evolution of a positive and negative linearly tapered undulator. In the positive taper we can see that some of the electrons are trapped inside the separatrix and they bunch, improving the energy exchange. In the negative taper case, we can see that electrons go around the separatrix, but we still have bunching and good extraction. For this last case, the taper will work well only when electron beam starts above resonance. Optimal taper occurs when approximately half of the electrons are trapped.

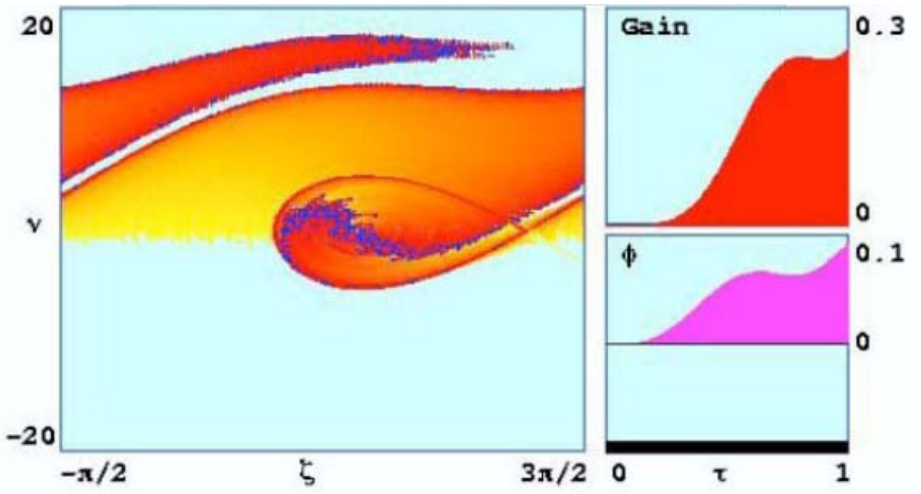

Figure 14. Phase space diagram of a positive linearly tapered undulator from [3].

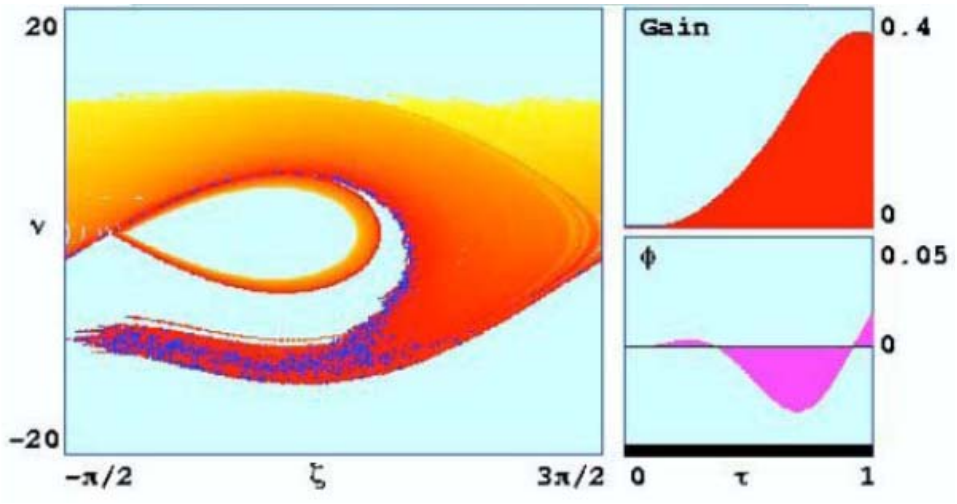

Figure 15. Phase space diagram of a negative linearly tapered undulator from [3].

Figures 16 and 17 show the phase space evolution of a positive and negative step-tapered undulator. There we can see that positive taper traps electrons like the positive linearly tapered case; and negative tapered electrons are similar to the negative linearly tapered case.

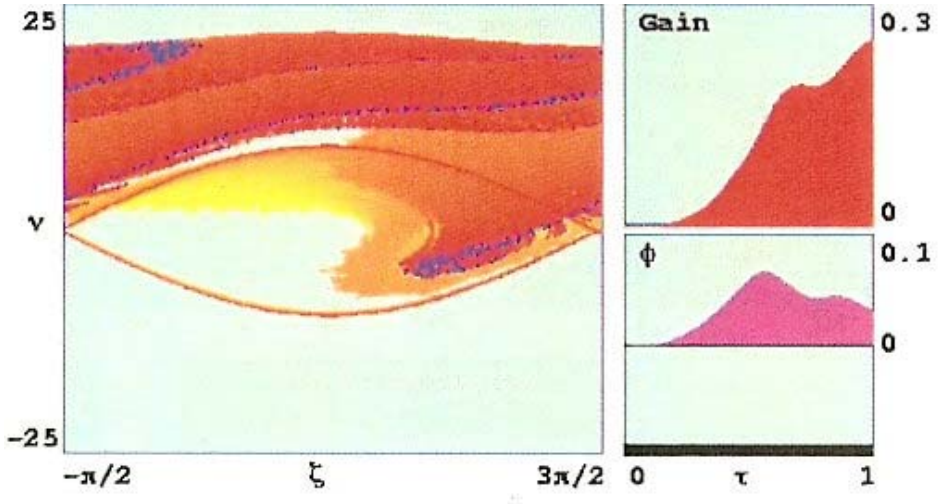

Figure 16. Phase space diagram of a positive step-tapered undulator from [3].

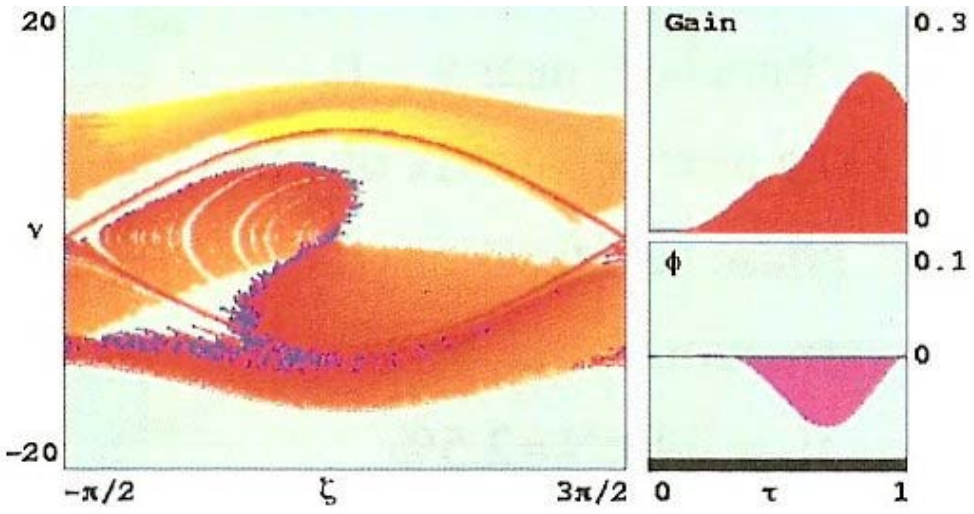

Figure 17. Phase space diagram of a negative step-tapered undulator from [3].

H. DIFFRACTION

Propagation of a laser beam can be described in free space by Maxwell's wave equation [7]

$$\left(\nabla^2 - \frac{1}{c^2}\frac{\partial^2}{\partial t^2}\right) a(\vec{x},t) = 0 \quad , \tag{III.24}$$

where $a(\vec{x},t)e^{i\alpha} = \left|a(\vec{x},t)\right| e^{i\phi a(\vec{x},t)} e^{i\alpha}$ is the optical electric field.

For laser light, the beam is coherent and the electric field is slow-varying in the direction of propagation over an optical wavelength and slow-varying in time over the optical frequency. In the last equation, α= kz-ωt represents the phase of the carrier wave, and the optical field is represented by a, as defined earlier.

If the optical field is constant, the electrical field describes a simple plane wave propagating in the z direction, containing only one frequency ω. If the wave's amplitude or phase contain spatial and time dependence the

laser beam will have a finite-with spectrum; if both dependences are slow then the laser will have a narrow spectrum. In an FEL, the amplitude and phase are slowly-varying, so we can make the following assumptions:

$$\frac{\partial|a|}{\partial t} \ll \omega|a| \ , \ \frac{\partial\phi}{\partial t} \ll \omega\phi \ , \ \frac{\partial|a|}{\partial z} \ll k|a| \ , \ \frac{\partial\phi}{\partial z} \ll k\phi \qquad \text{(III.25)}$$

After substitutions we get

$$\left[\vec{\nabla}_\perp^2 a + \left(\frac{\partial^2 a}{\partial z^2} + 2ik\frac{\partial a}{\partial z} - k^2 a\right) - c^{-2}\left(\frac{\partial^2 a}{\partial t^2} - 2i\omega\frac{\partial a}{\partial t} - \omega^2 a\right)\right] e^{i\alpha} = 0 \qquad \text{(III.26)}$$

Using assumptions (III.25), we can neglect the terms with two derivatives. Multiplying by $e^{-i\alpha}$ and using ω=kc we arrive at

$$\left[\vec{\nabla}_\perp^2 + 2ik\left(\frac{\partial}{\partial z} + \frac{1}{c}\frac{\partial}{\partial t}\right)\right] a(\vec{x},t) = 0 \ . \qquad \text{(III.27)}$$

This equation can be simplified further by introducing a coordinate transformation u=z-ct and a dimensionless time τ=ct/L where L is the length of the undulator. Then, the wave equation can be written with one less partial derivative,

$$\left[\vec{\nabla}_\perp^2 + \frac{2ik}{L}\frac{\partial}{\partial\tau}\right] a(\vec{x},t) = 0 \ , \ \text{or} \qquad \text{(III.28)}$$

$$\left[\frac{-iL}{2k}\vec{\nabla}_\perp^2 + \frac{\partial}{\partial\tau}\right] a(\vec{x},t) = 0 \ . \qquad \text{(III.29)}$$

This equation is known as the parabolic wave equation. The first term in this equation is the diffraction term, and its magnitude depends on the transverse area of the laser beam, the wavelength (λ=2π/k), and the undulator length L.

The Rayleigh length Z_0 (distance from the mode waist to where the area of the optical mode doubles due to diffraction) relates the optical mode waist radius W_0 to

the wavelength of the light by $Z_0 = \pi W_0^2 / \lambda$. In dimensionless units $z_0 = Z_o / L$. Based on diffraction along the undulator, so $Z_o \approx L$, the characteristic mode waist radius is $\sqrt{L\lambda/\pi} = \sqrt{2L/k}$. If the optical mode radius is much larger than $\sqrt{L\lambda/\pi}$, then the diffraction has a small effect over the undulator. If it is smaller, diffraction has a big effect on propagation, changing both the amplitude and phase of the optical field.

It is important to mention that this description of diffraction is calculated for laser light in free space. For an FEL in the amplifier configuration, diffraction is altered by the electron interaction. Inside the undulator, the wave equation is inhomogeneous, and the Gaussian distribution of the optical field changes; the laser beam is affected by the electrons that try to focus the laser beam. Then we have to consider the last term of the FEL wave equation $< -je^{-i\zeta} >$. This new term affects the diffraction of the optical field.

I. SHORT PULSES AND SLIPPAGE

For energy exchange between the electrons and optical field, they must overlap inside the undulator. During their pass through the wiggler, electrons and photons have different velocities. Photons travel at speed of light, and relativistic electrons move close to it but slower. The term used to describe the overlap of the optical and electron pulses is known as "slippage"; according to the resonance condition, the electrons drop behind the light by a slippage distance Nλ over the length of the undulator. Figure 18 shows the slippage concept. Red pulse is the electron pulse

and blue pulse is the optical pulse; the left overlap represents the position at the beginning of the undulator, and the right overlap is at the end of the undulator.

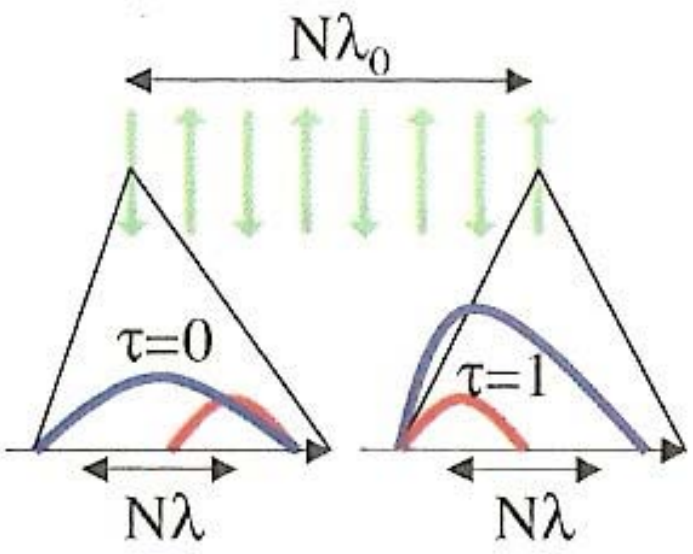

Figure 18. Electron and light slippage from [3].

We have short pulses when the micropulse length l_e is on the order of or less than the slippage distance Nλ. In order to get the required energy transfer, the short electron pulses and optical pulses must be synchronized. That process develops in stages, and electron bunching must take place in the right moment. At the beginning of the undulator the electrons and light overlap, but there is no bunching and therefore no gain. At the middle, electrons during their bunching process slightly amplify the light pulse. At the end, bunched electrons amplify the trailing part of the optical pulse. As a result, the optical pulse

centroid travels slower than speed of light; this process is called “optical lethargy”. Figure 19 shows this process.

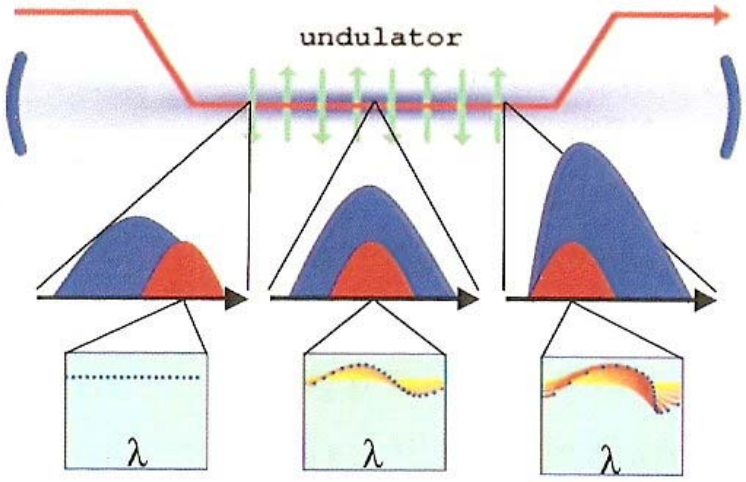

Figure 19. Optical lethargy from [3].

IV. SIMULATIONS OF FREE ELECTRON LASERS IN AMPLIFIER CONFIGURATION

In this chapter, several free electron laser amplifiers were explored with computer simulations, using the NPS Apple Xserve cluster with 64 nodes/128 processors. On this device, a simulation program was run that solved the coupled pendulum and FEL wave equations in order to understand the four dimensional behavior of the high power FEL amplifier. The simulation program required dimensionless input parameters, which make the results applicable to a broad range of FELs.

A. DESCRIPTION OF THE INITIAL PARAMETERS

The first step in this process is to establish the initial parameters that describe the system to be evaluated. Using these parameters, the dimensionless input variables are calculated in order to run the simulation.

We can classify these parameters as primary and secondary. Secondary parameters are coupled to the primary parameters and they have to be calculated using several formulas that will be described in this work.

The desired characteristics of the device were introduced into an Excel spread sheet, which calculated the secondary parameters using formulas, and the dimensionless input parameters for the simulation program. Tables 1, 2 and 3 show the description of the dimensional parameters that were used and the formulae used to obtain the secondary dimensional parameters.

	UNDULATOR PARAMETERS	
λ_0	Undulator period	
N	Number of periods	
g	Undulator gap	
B	Magnetic field (rms)	
K	Undulator parameter	$K = eB\lambda_0 / 2\pi mc^2$
L	Undulator length	$L = N\lambda_0$

Table 1. Undulator parameters used to describe an FEL in a simulation.

	ELECTRON BEAM PARAMETERS	
E_b	Beam kinetic energy	
q_b	Bunch charge	
r_b	Beam radius (rms)	$r_{b=}\sqrt{\varepsilon_n L / 4\gamma}$
t_b	Pulse duration, FWHM	
Ω	Pulse repetition frequency	
l_b	Pulse length, FWHM	$l_b = t_b c$
γ	Lorentz factor	$\gamma = (E_b + 0.511MeV) / 0.511MeV$
I_{Peak}	Peak current	$I_{Peak} = q_b / t_b$
I_{Avg}	Average current	$I_{Avg} = q_b \Omega$
ε_n	Normalized rms emittance	
ε_l	Longitudinal emittance	
$\frac{\Delta\gamma}{\gamma}$	Beam energy spread (rms)	$\frac{\Delta\gamma}{\gamma} = 2.35\varepsilon_l / (E_b)(t_b)$
$\Delta\theta$	Beam angular spread (rms)	$\Delta\theta = \varepsilon_n / \gamma r_b$
P_b	Beam average power	$P_b = E_b I_{Avg}$

Table 2. Electron beam parameters used to describe an FEL in a simulation.

	OPTICAL PARAMETERS	
P_{in}	Seed laser power	
T_{in}	Seed pulse duration	
S	Distance to First Optic	
Z_0	Rayleigh length	$Z_0 = \pi W_0^2 / \lambda$
λ	Optical wavelength	$\lambda = \lambda_0 (1+K^2) / 2\gamma^2$
W_0	Mode waist radius, 1/e	$W_0 = \sqrt{4 r_b^2 / F}$

Table 3. Optical parameters used to describe an FEL in a simulation.

B. SIMULATIONS OF THE FIRST FEL

This first laser was intended to have a power of 100 kW with a wavelength of 1.6 μm in an amplifier configuration. The undulator has 120 periods, and its length is 324 cm. Tables 4 through 7 show these parameters.

	ELECTRON BEAM PARAMETERS	
E_b	Beam energy (MeV)	80
q_b	Bunch charge (nC)	0.2
r_b	Beam radius, (mm)	0.13
t_b	Pulse duration, FWHM (ps)	1.0
Ω	Pulse rep frequency (MHz)	703
l_b	Pulse length, FWHM (cm)	0.03
γ	Lorentz factor	158
I_{Peak}	Peak current (A)	200
I_{Avg}	Average current (mA)	141
ε_n	Normalized rms emittance (mm mrad)	3.5
ε_l	Longitudinal emittance (keV ps)	36
$\Delta\gamma / \gamma$	Beam energy spread (%)	0.11
$\Delta\theta$	Beam angular spread (mrad)	0.17
P_b	Beam average power (MW)	11

Table 4. Initial electron beam parameters of the first simulated FEL device.

UNDULATOR PARAMETERS		
λ_0	Undulator period (cm)	2.7
N	Number of periods	120
g	Undulator gap (cm)	1.00
K	Undulator parameter, rms	1.39
L	Undulator length (cm)	324

Table 5. Initial undulator parameters of the first simulated FEL device.

OPTICAL PARAMETERS		
P_{in}	Seed laser power (W)	100
T_{in}	Seed pulse duration, FWHM (ps)	2.0
S	Distance to First Optic (cm)	1000
Z_0	Rayleigh length (cm)	28
λ	Optical wavelength (microns)	1.6
W_0	Mode waist radius, 1/e (mm)	0.38

Table 6. Initial optical parameters of the first simulated FEL device.

DIMENSIONLESS PARAMETERS		
j	Normalized current density, linear undulator	3356
σ	Normalized beam radius	0.10
σ_t	Normalized beam angular spread	0.42
σ_{vg}	Phase velocity spread due to energy spread	1.6
σ_z	Normalized pulse length	1.6
a_0	Normalized initial optical field amplitude	5.4
σ_a	Normalized initial optical pulse length	3.1
z_0	Normalized Rayleigh length	0.09
w_0	Normalized mode waist radius	0.30
ω_β	Betatron oscillation frequency	6.7

Table 7. Dimensionless parameters of the first simulated FEL device.

The first parameter to analyze was the taper start time τ_s. This time is established as a dimensionless parameter using a scale from 0 to 1, with $\tau_s = 0$ corresponding to the beginning of the undulator and $\tau_s = 1$ the end of he undulator. The taper start time was simulated for several values from 0.4 to 0.8 with intervals of 0.1; using a taper rate of δ=40π. The start time with the greatest extraction was at $\tau_s = 0.7$ with an extraction η = 0.92%. Figure 20 shows a graph of the obtained extractions versus the simulated taper start times for δ=40π.

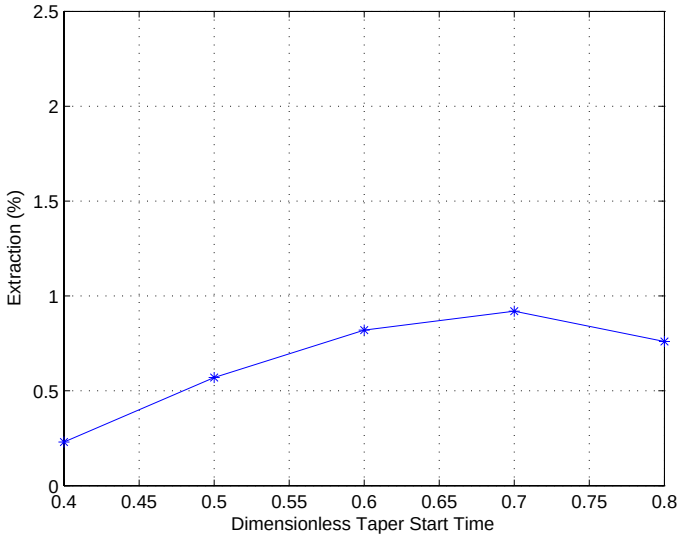

Figure 20. Graph of extraction vs. taper start times.

The full simulation output for the most efficient taper start time ($\tau_s = 0.7$) at δ=40π is shown on Figure 21. There we can see the power P(τ) growing to saturation at the end of the undulator (τ=1), with about half the electrons trapped in phase space (ζ,ν) as shown on phase space diagram. Also

we can see a typical diffraction pattern of the beam in x and y. Slippage produces a narrow optical pulse in the *z* direction.

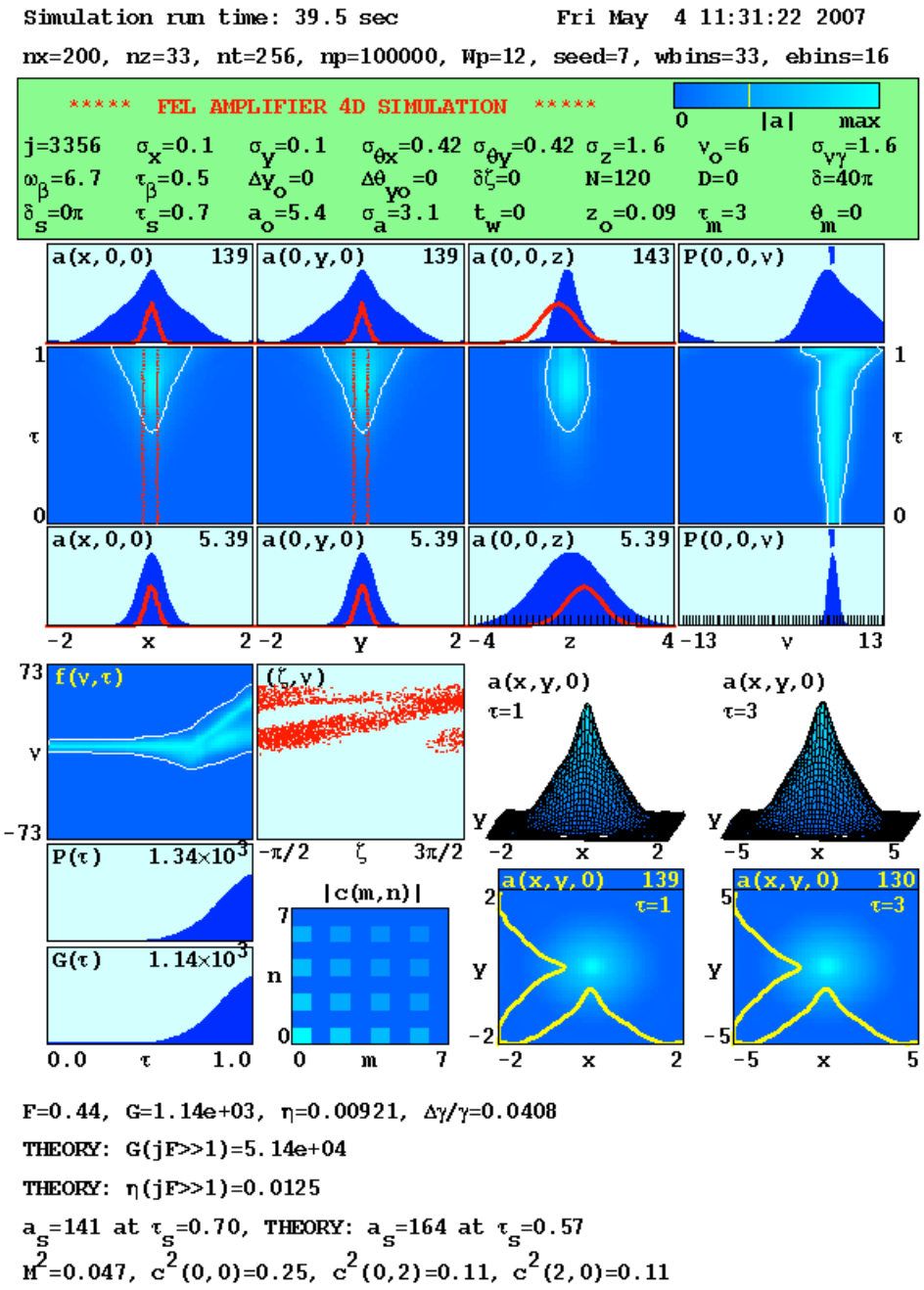

Figure 21. Full simulation output for taper start time 0.7.

Once the most efficient value of the taper start time ($\tau_s = 0.7$) was found, it was used to run a set of simulations to analyze the dimensionless linear taper rate (δ). Simulations were run for δ values from 0 to 80π at intervals of 10π. The most efficient rate was at δ = 40π with an extraction η = 0.92%. Figure 22 shows a graph of the obtained extractions versus simulated taper rates.

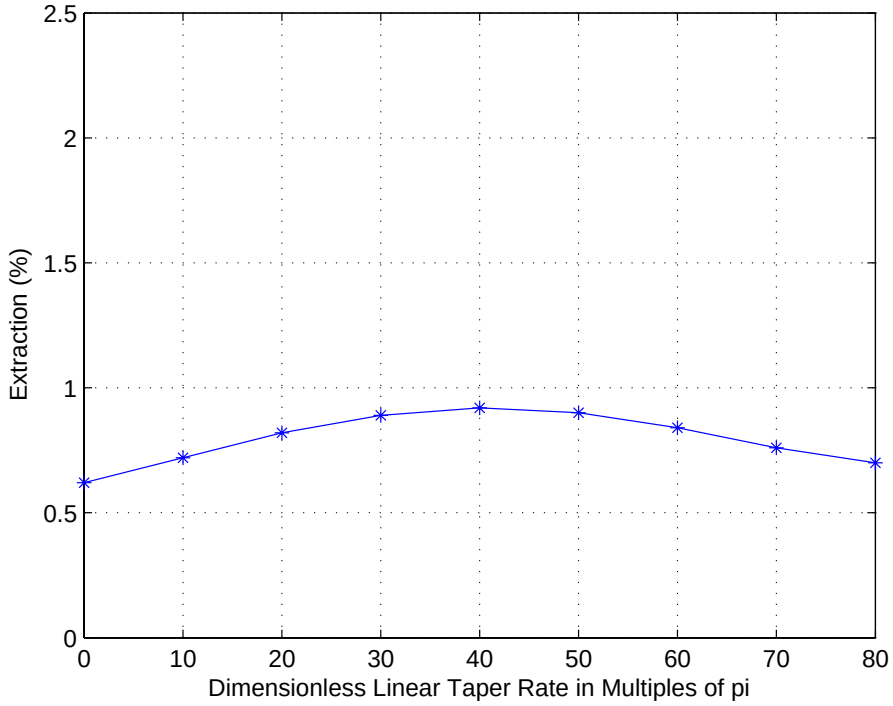

Figure 22. Graph of extraction vs. linear taper rates.

The full simulation output for the most efficient taper start time ($\tau_s = 0.7$) is shown in Figure 21 (coincidently the taper rate used in that simulation was the most efficient). The results are the same as the previous simulation. Since the extraction is not enough to achieve 100 kW, it is necessary to change other parameters in order to reach the goal.

In order to look for a better extraction, a longer undulator was tried, increasing the number of periods to 140. Since the length of the undulator changed to 378 cm, it was necessary to calculate the dimensionless input parameters again. Table 8 shows only the parameters that changed for this case.

	ELECTRON BEAM PARAMETERS	
r_b	Beam radius, (mm)	0.14
$\Delta\theta$	Beam angular spread (mrad)	0.15
	UNDULATOR PARAMETERS	
N	Number of periods	140
L	Undulator length (cm)	378
	OPTICAL PARAMETERS	
W_0	Mode waist radius, 1/e (mm)	0.41
	DIMENSIONLESS PARAMETERS	
j	Normalized current density, linear undulator	4568
σ_{vg}	Phase velocity spread due to energy spread	1.9
σ_z	Normalized pulse length	1.3
a_0	Normalized initial optical field amplitude	6.9
σ_a	Normalized initial optical pulse length	2.7
ω_β	Betatron oscillation frequency	7.8

Table 8. New parameters for N=140.

Using a taper start time $\tau_s = 0.5$, a set of simulations explored the effect of the dimensionless taper rate (δ). Simulations were run for δ values from 0 to 80π at intervals of 10π. The most efficient rate was at δ = 30π with an extraction η = 1.13%. Figure 23 shows a graph of obtained extractions versus the simulated taper rates.

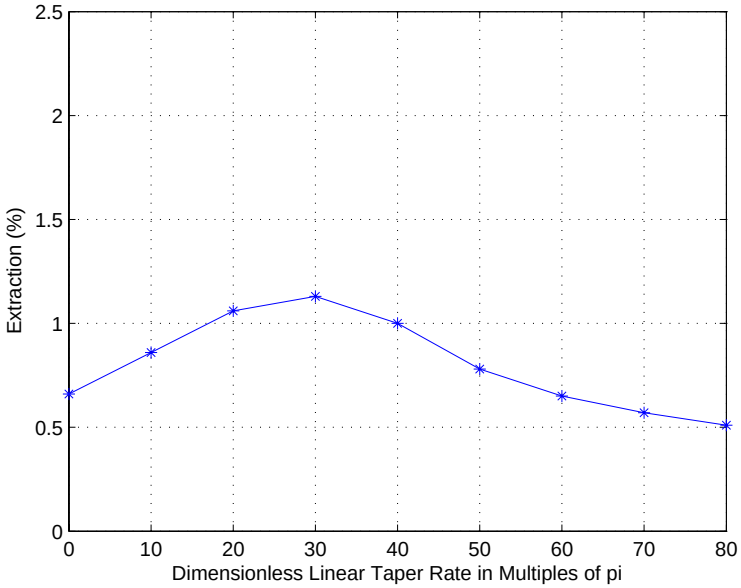

Figure 23. Graph of extraction vs. linear taper rates for N=140.

With this longer undulator we can see that the extraction is bigger even with a smaller taper rate. Diffraction patterns are very similar to the previous case and a higher power reaches saturation at the end of the undulator. On Figure 24 we can see that electron bunching is quite similar to the previous case, but the optical field evolved into a combination of higher-order modes.

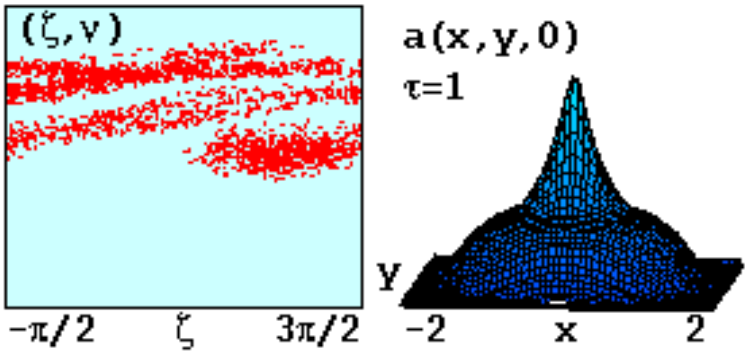

Figure 24. Electron bunching and optical field for linear taper rate δ=30π.

Continuing with this exploration, and using the optimal taper rate found for this FEL (δ=30π) and a taper start time $\tau_s = 0.6$, this device was analyzed by changing the electron beam pulse duration (t_b) in a range from 0.4 to 1.6 ps in 0.2 ps steps. It is important to mention that any change in this parameter changes the input parameters of the simulation, so a recalculation of dimensionless parameters was made for every value of t_b. The largest extraction (η = 1.18%) was found at $t_b = 0.8$ps. Figure 25 shows a graph of the obtained extractions versus the simulated electron beam pulse duration.

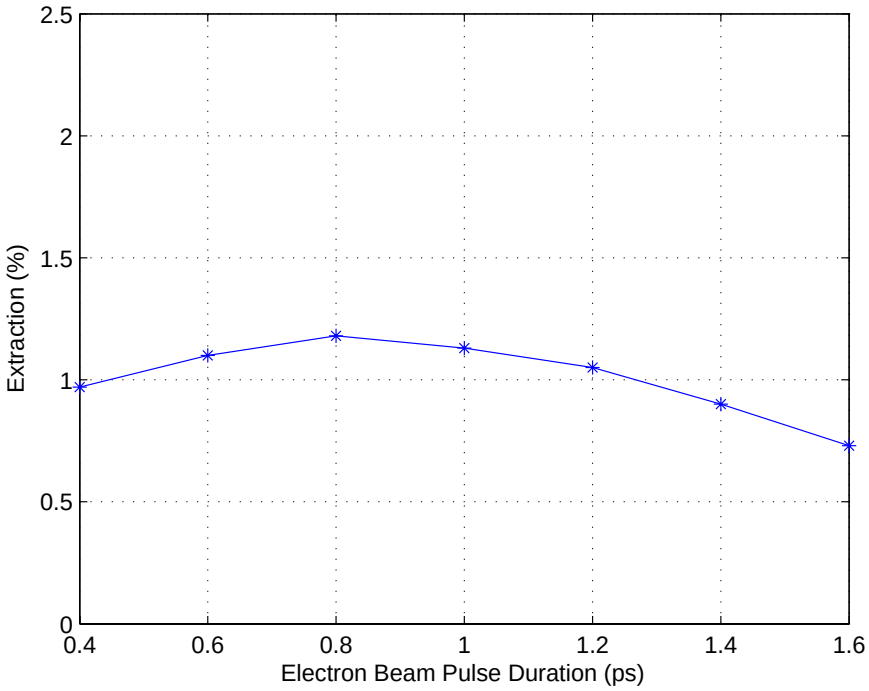

Figure 25. Graph of extraction vs. electron beam pulse duration.

The results at the best pulse duration ($t_b = 0.8$ ps) are similar to the last case, but this time it did not have many higher-order optical modes.

The next step is to change other parameters to obtain a better extraction. This time the bunch charge was changed from 0.2 to 0.4 nC, with the pulse repetition frequency cut in half ($\Omega = 350$ MHz) to keep the average current the same (140 mA). This change affects some of the input parameters to the simulation program, so, it is necessary to recalculate the dimensionless parameters to create another input file. Table 9 shows the initial parameters that changed for this new case with respect to the last case upon changing the bunch charge value.

ELECTRON BEAM PARAMETERS		
q_b	Bunch charge (nC)	0.4
Ω	Pulse rep frequency (MHz)	350
I_{Peak}	Peak current (A)	400
I_{Avg}	Average current (mA)	140
ε_l	Longitudinal emittance (keV ps)	38

DIMENSIONLESS PARAMETERS		
j	Normalized current density, linear undulator	9137
σ_{vg}	Phase velocity spread due to energy spread	2.0
a_0	Normalized initial optical field amplitude	9.7

Table 9. Parameters that changed for micropulse charge of 0.4

Using these new parameters the input file was updated for the simulation, and several runs tried to obtain optimal outputs for the same ranges of taper values.

Again the first parameter to analyze was the taper start time. The taper start time was simulated for several values from 0.4 to 0.8 at intervals of 0.1; using a linear taper rate of 40π. The optimum start time was at 0.5 with an extraction η = 2.06%. Figure 27 shows a graph of the obtained extractions versus the simulated taper times.

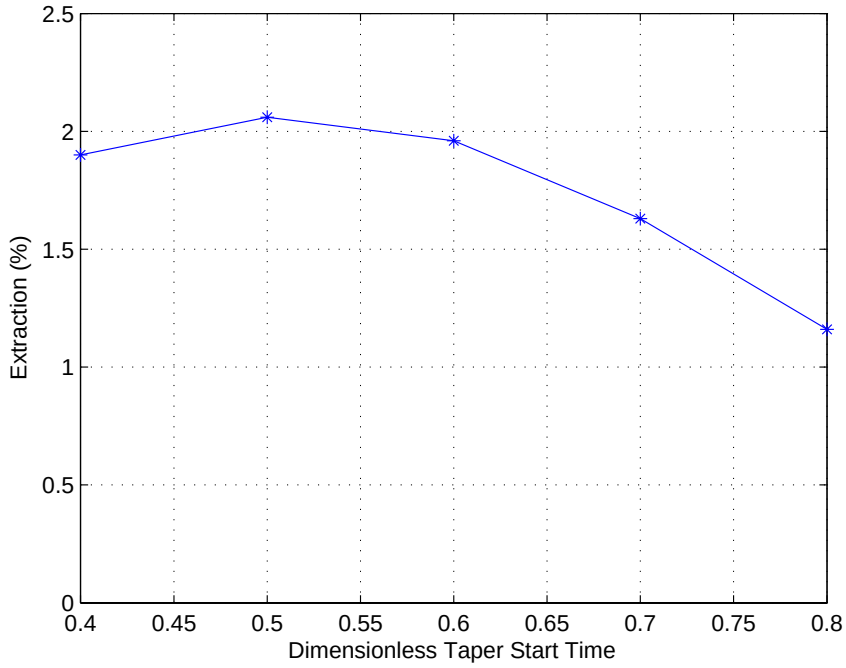

Figure 26. Extraction vs. dimensionless taper start time for micropulse charge of 0.4 nC.

The results for the optimum taper time (0.5) are very similar to the last case, but this there was slightly better electron bunching, resulting in a better extraction. As a result and a higher power was delivered when saturation was reached at the end of the undulator.

Again, once the optimum value of the taper start time (0.5) was found, it was used to run a set of simulations to analyze the dimensionless taper rate (δ). Simulations were run for δ values from 0 to 80π at intervals of 10π. The optimum rate was at δ = 60π and δ = 70π with an extraction η = 2.32%. Figure 29 shows a graph of the obtained extractions versus the simulated taper rates.

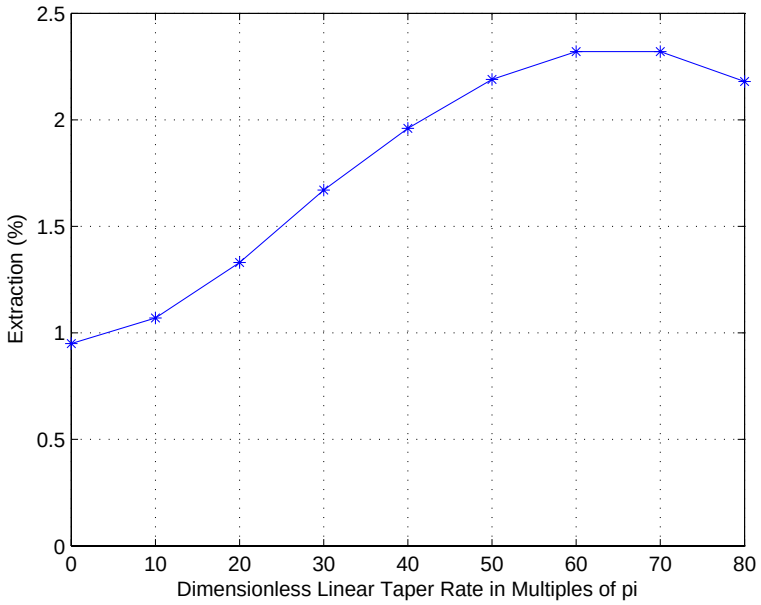

Figure 27. Extraction vs. dimensionless taper rates for micropulse charge of 0.4 nC.

The results for the taper rate δ = 60π are shown in Figure 28. Extraction is much better in this case, but the taper rate must be large in order to reach this level of extraction. As in the last case, a higher power was delivered when saturation was reached at the end of the undulator. It may be possible to reach these levels changing other parameters.

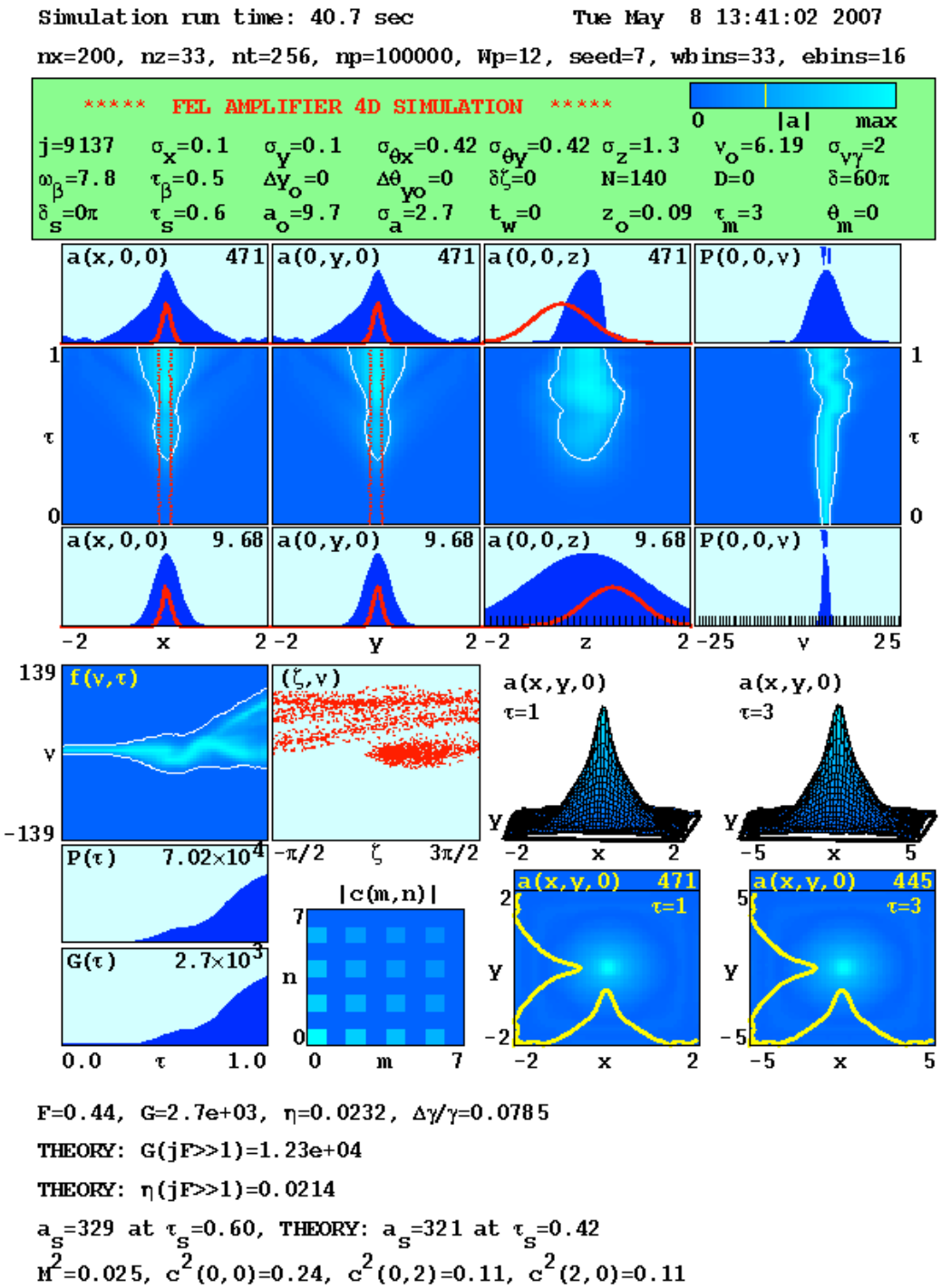

F=0.44, G=2.7e+03, η=0.0232, Δγ/γ=0.0785

THEORY: G(jF>>1)=1.23e+04

THEORY: η(jF>>1)=0.0214

a_s=329 at τ_s=0.60, THEORY: a_s=321 at τ_s=0.42

M^2=0.025, $c^2(0,0)$=0.24, $c^2(0,2)$=0.11, $c^2(2,0)$=0.11

Figure 28. Results for micropulse charge of 0.4 nC and taper rate δ=60π.

The last explored parameter was the emittance; this parameter is mainly determined by the injector. Emittance changes have a direct effect on the initial parameters; and any change of this parameter needs to be applied to the spread sheet in order to calculate the new input parameters.

For this simulation, emittance was adjusted to 5.1 mm mrad, and Table 10 shows the initial parameters that changed for this new case with respect to the last case upon changing emittance.

	ELECTRON BEAM PARAMETERS	
ε_n	Normalized rms emittance (mm mrad)	5.1
$\Delta\theta$	Beam angular spread (mrad)	0.23
	OPTICAL PARAMETERS	
W_0	Mode waist radius, 1/e (mm)	0.40
	DIMENSIONLESS PARAMETERS	
j	Normalized current density, linear undulator	9786
σ_t	Normalized beam angular spread	0.63
a_0	Normalized initial optical field amplitude	10.0
z_0	Normalized Rayleigh length	0.08
w_0	Normalized mode waist radius	0.29

Table 10. Parameters that changed after changing the emittance.

With these parameters and using a taper start time $\tau_s = 0.5$, it was run a set of simulations to explore the dimensionless taper rate (δ). Simulations were run for δ values from 30π to 80π at intervals of 10π. The optimum taper rate was at δ = 60π with an extraction η = 2.15%. Figure 29 shows a graph of obtained extractions versus the simulated taper rates.

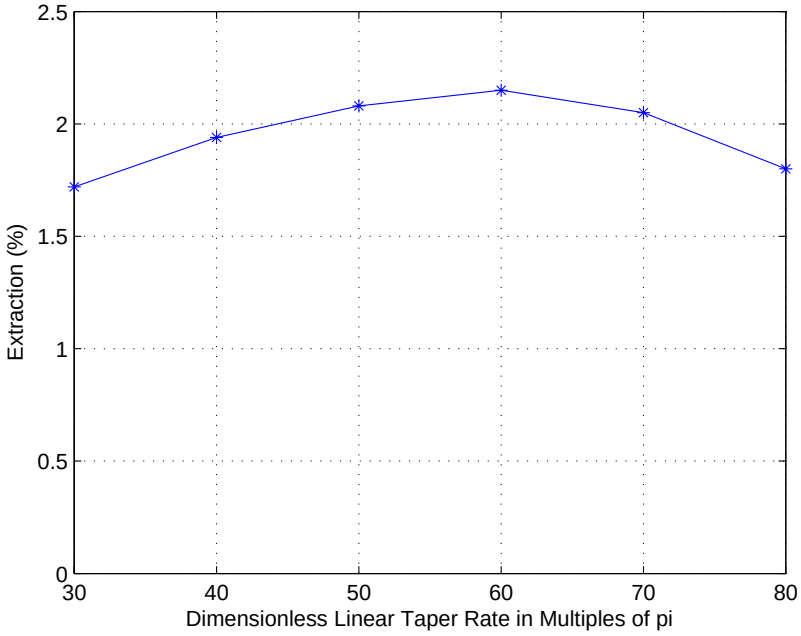

Figure 29. Extraction vs. dimensionless taper rates for emittance=5.1mm mrad.

This graph shows that with this value of emittance, taper rate variation over this range does not have a big effect on the extraction. For $\delta = 60\pi$, the results of the simulation are very similar to the last case. As in the last case, a higher power was delivered when saturation was reached at the end of the undulator.

C. SIMULATIONS OF THE SECOND FEL

This second set of simulations explores an FEL amplifier with a power of 1 megawatt and an optical wavelength of 1.6 microns. The same procedure is used for this laser, but this time the number of periods of the undulator was analyzed for several values in order to find the optimum. The general input parameters of this device are shown on Tables 11, 12, 13 and 14.

ELECTRON BEAM PARAMETERS		
E_b	Beam energy (MeV)	75.5
q_b	Bunch charge (nC)	1.5
r_{bx}	Beam radius, x (mm)	0.31
r_{by}	Beam radius, y (mm)	0.18
t_b	Pulse duration, FWHM (ps)	1.1
Ω	Pulse rep frequency (MHz)	703
l_b	Pulse length, FWHM (cm)	0.034
γ	Lorentz factor	149
I_{Peak}	Peak current (A)	1333
I_{Avg}	Average current (mA)	1055
ε_{nx}	Normalized rms emittance, x (mm mrad)	15.0
ε_{ny}	Normalized rms emittance, y (mm mrad)	5.0
ε_l	Longitudinal emittance (keV ps)	70
$\frac{\Delta\gamma}{\gamma}$	Beam energy spread (%)	0.19
$\Delta\theta_x$	Beam angular spread, x (mrad)	0.32
$\Delta\theta_y$	Beam angular spread, y (mrad)	0.18
P_b	Beam average power (MW)	80

Table 11. Initial electron beam parameters of the second simulated FEL.

UNDULATOR PARAMETERS		
λ_0	Undulator period (cm)	2.62
N	Number of periods	150
g	Undulator gap (cm)	1.00
K	Undulator parameter, rms	1.30
L	Undulator length (cm)	393

Table 12. Initial undulator parameters of the second simulated FEL device.

OPTICAL PARAMETERS		
P_{in}	Seed laser power (W)	100
T_{in}	Seed pulse duration, FWHM (ps)	2.3
S	Distance to First Optic (cm)	1000
Z_0	Rayleigh length (cm)	105
λ	Optical wavelength (microns)	1.59
W_0	Mode waist radius, 1/e (mm)	0.73

Table 13. Initial optical parameters of the second simulated FEL device.

DIMENSIONLESS PARAMETERS		
j	Normalized current density, linear undulator	20288
σ_x	Normalized beam radius, x	0.22
σ_y	Normalized beam radius, y	0.13
σ_{tx}	Normalized beam angular spread, x	0.89
σ_{ty}	Normalized beam angular spread, y	0.52
σ_{vg}	Phase velocity spread due to energy spread	3.7
σ_z	Normalized pulse length	1.4
a_0	Normalized initial optical field amplitude	4.3
σ_a	Normalized initial optical pulse length	2.8
z_0	Normalized Rayleigh length	0.27
w_0	Normalized mode waist radius	0.52
ω_β	Betatron oscillation frequency	8.2

Table 14. Dimensionless parameters of the second simulated FEL device.

For the first simulation, it was necessary to update the dimensionless input file for each value of N. The number of periods was analyzed from N=100 through N=200 at intervals of 10, obtaining the highest extraction η = 2.21% at N=140. Figure 30 shows a graph of the extraction versus the number of periods of the undulator.

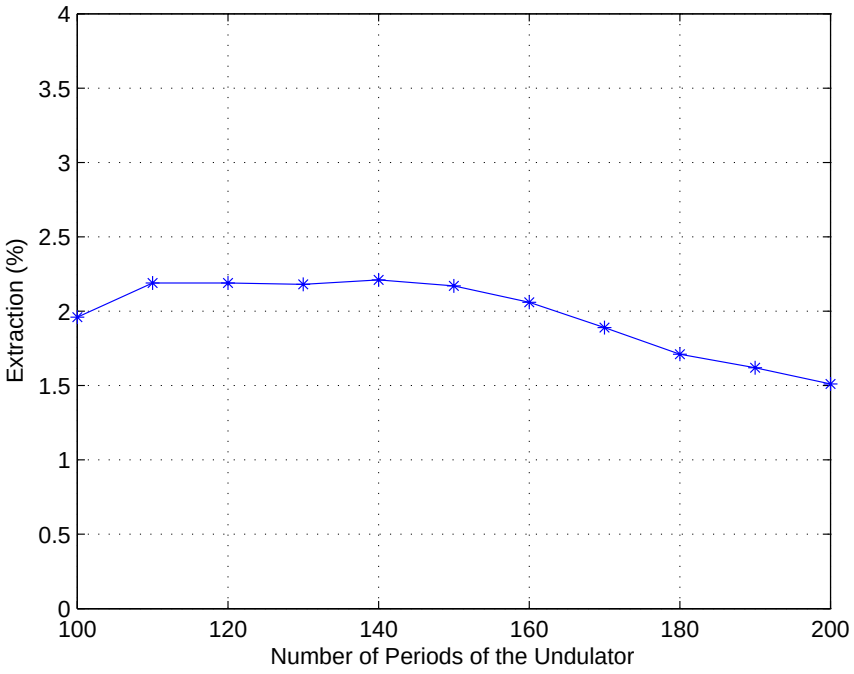

Figure 30. Extraction vs. number of periods of the second FEL.

Figure 31 shows the results of the simulation for this set of parameters with N=140, which is the optimum value.we can see the power P(τ) growing to saturation at the end of the undulator (τ=1) with an intermediate bump corresponding to a synchrotron oscillation, and about half the electrons trapped in phase space (ζ,ν) as shown on phase space diagram.

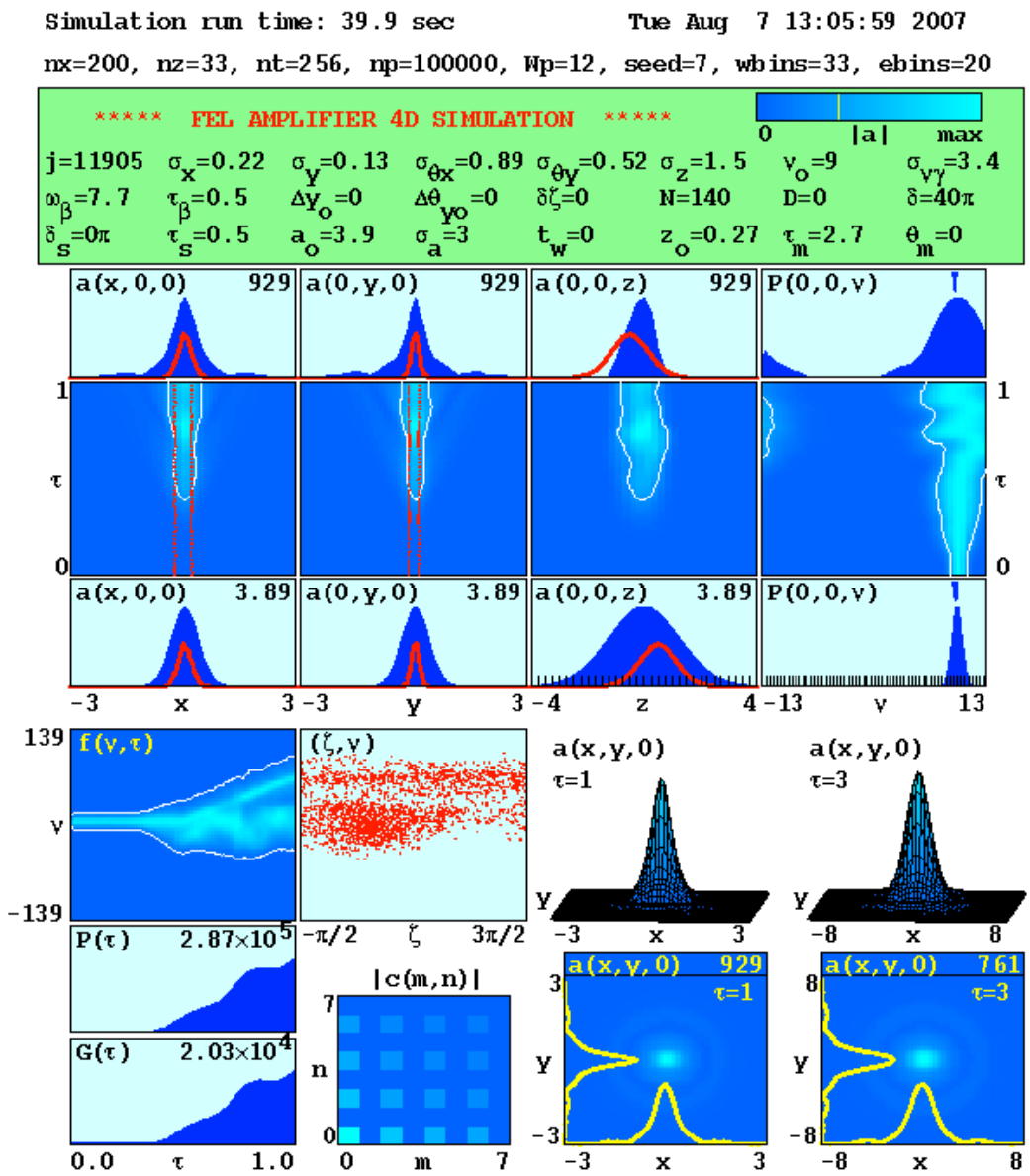

F=0.42, G=2.03e+04, η=0.0221, Δγ/γ=0.0954

THEORY: G(jF>>1)=2.65e+04

THEORY: η(jF>>1)=0.0179

a_s=535 at τ_s=0.50, THEORY: a_s=371 at τ_s=0.48

M^2=0.058, $c^2(0,0)$=0.33, $c^2(2,0)$=0.13, $c^2(0,2)$=0.12

Figure 31. Results for N=140 of the second FEL.

Using the undulator with N=140, the taper start time was simulated for several values from 0.0 to 0.9 at intervals of 0.1 with a taper rate of 40π. The optimum start time (greatest extraction) was at 0.5 with an extraction η = 2.21%. Figure 32 shows a graph of the obtained extractions versus the simulated taper times.

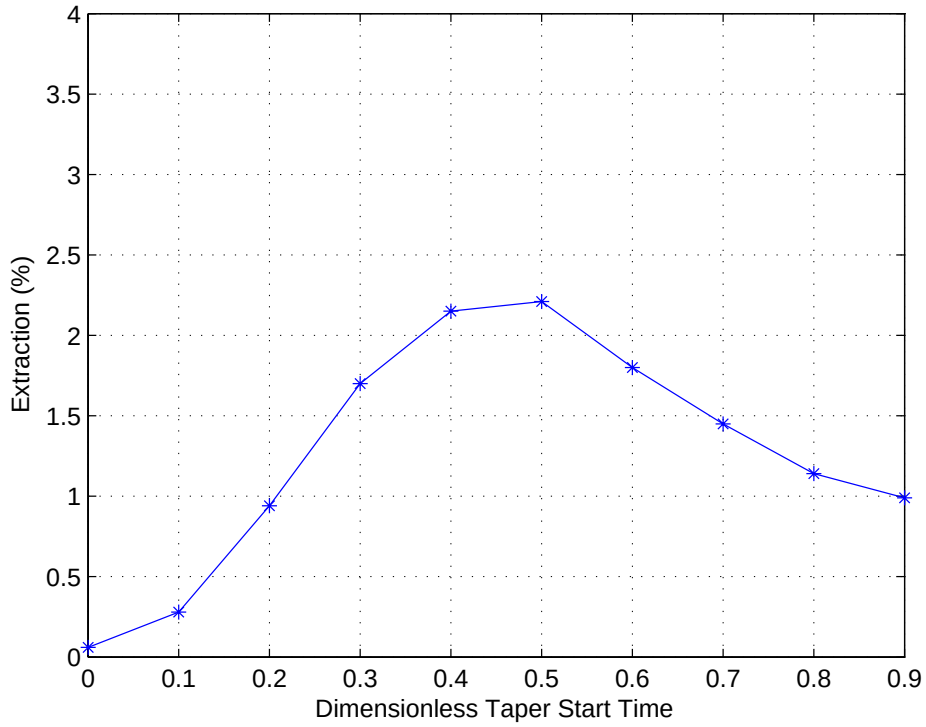

Figure 32. Extraction vs. dimensionless taper start time of the second FEL.

The results for the best taper time (0.5) are shown in Figure 31.

The taper start time of 0.5 was used to run a set of simulations to analyze the dimensionless taper rate (δ). Simulations were run for δ values from 0 to 150π at intervals of 10π. The optimum rate was at δ = 100π with an

extraction η = 3.55%. Figure 33 shows a graph of the obtained extractions versus the taper rates.

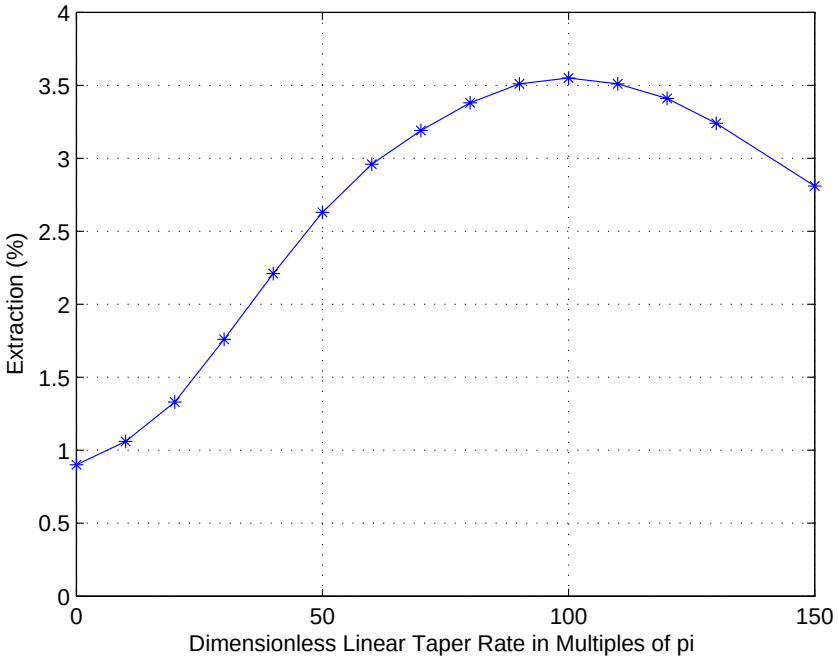

Figure 33. Extraction vs. dimensionless linear taper rates of the second FEL.

The results for the optimum taper rate δ = 100π are shown in Figure 34. Extraction is much better in this case. As in the last case, a higher power was delivered when saturation was reached at the end of the undulator. Less than half of the electrons bunched inside of the separatrix as shown on the phase space diagram.

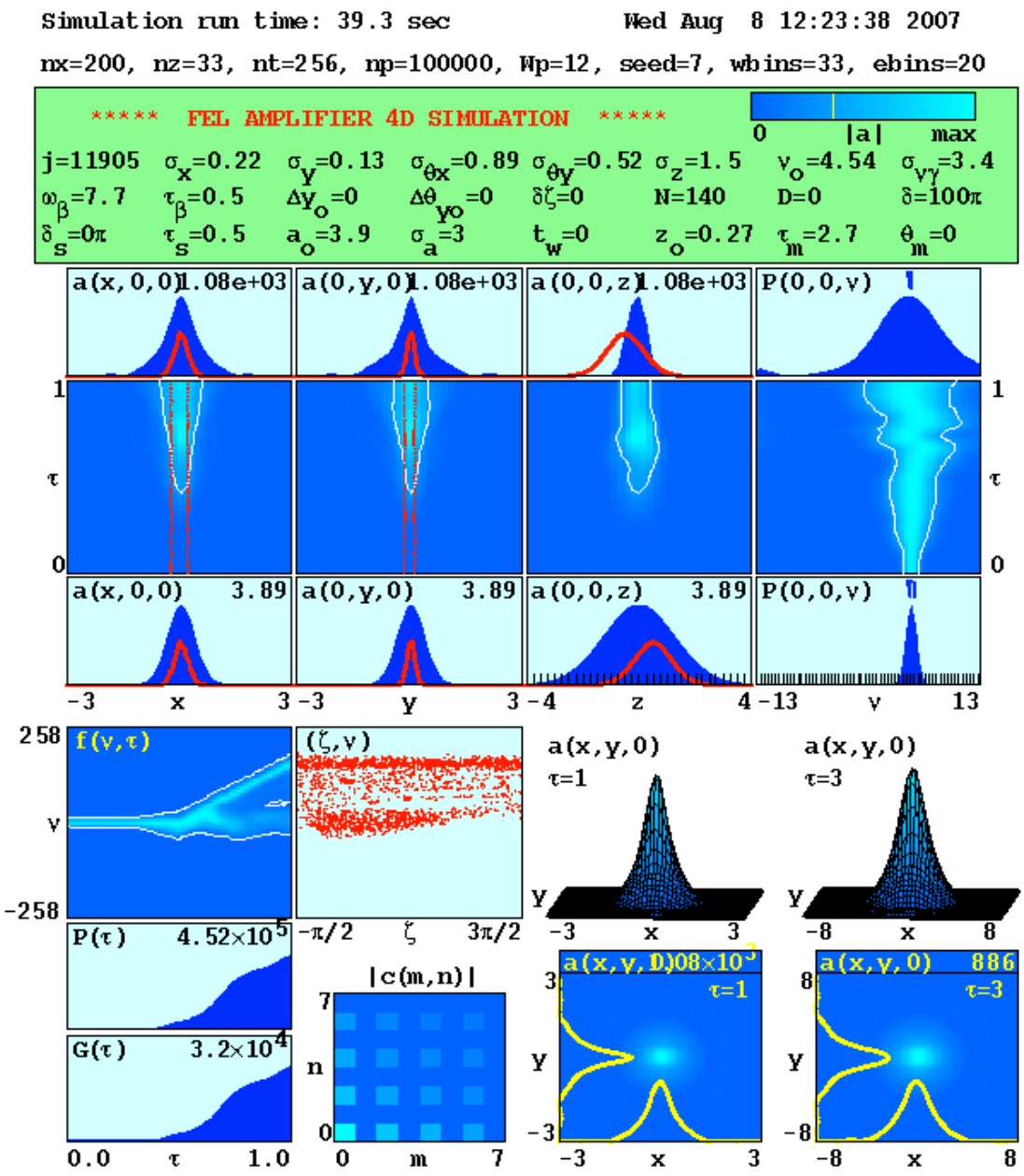

F=0.42, G=3.2e+04, η=0.0355, Δγ/γ=0.139

THEORY: G(jF>>1)=6.01e+04

THEORY: η(jF>>1)=0.0446

a_s=489 at τ_s=0.50, THEORY: a_s=371 at τ_s=0.48

M^2=0.094, $c^2(0,0)$=0.35, $c^2(2,0)$=0.14, $c^2(0,2)$=0.12

Figure 34. Results for δ = 100π of the second FEL.

D. SIMULATIONS OF THE THIRD FEL

This third set of simulations explores an FEL amplifier with a power of 3 megawatts and an optical wavelength of 1.6 microns. In this case, more realistic electron beam parameters were generated by an external computer program (Parmela). The number of periods of the undulator was adjusted in order to obtain the most extraction. The general input parameters of this device are shown on Tables 15 through 18.

	ELECTRON BEAM PARAMETERS	
E_b	Beam energy (MeV)	75.5
q_b	Bunch charge (nC)	1.5
r_{bx}	Beam radius, x (mm)	0.28
r_{by}	Beam radius, y (mm)	0.18
t_b	Pulse duration, FWHM (ps)	0.88
Ω	Pulse rep frequency (MHz)	703
l_b	Pulse length, FWHM (cm)	0.026
γ	Lorentz factor	149
I_{Peak}	Peak current (A)	1705
I_{Avg}	Average current (mA)	1055
ε_{nx}	Normalized rms emittance, x (mm mrad)	14.0
ε_{ny}	Normalized rms emittance, y (mm mrad)	5.6
ε_l	Longitudinal emittance (keV ps)	60
$\frac{\Delta\gamma}{\gamma}$	Beam energy spread (%)	0.21
$\Delta\theta_x$	Beam angular spread, x (mrad)	0.33
$\Delta\theta_y$	Beam angular spread, y (mrad)	0.21
P_b	Beam average power (MW)	80

Table 15. Initial electron beam parameters of the third simulated FEL.

UNDULATOR PARAMETERS		
λ_0	Undulator period (cm)	2.62
N	Number of periods	130
g	Undulator gap (cm)	1.00
K	Undulator parameter, rms	1.30
L	Undulator length (cm)	341

Table 16. Initial undulator parameters of the third simulated FEL device.

OPTICAL PARAMETERS		
P_{in}	Seed laser power (W)	100
T_{in}	Seed pulse duration, FWHM (ps)	1.76
S	Distance to First Optic (cm)	1000
Z_0	Rayleigh length (cm)	89
λ	Optical wavelength (microns)	1.59
W_0	Mode waist radius, 1/e (mm)	0.67

Table 17. Initial optical parameters of the third simulated FEL device.

DIMENSIONLESS PARAMETERS		
j	Normalized current density, linear undulator	12836
σ_x	Normalized beam radius, x	0.14
σ_y	Normalized beam radius, y	0.22
σ_{tx}	Normalized beam angular spread, x	0.55
σ_{ty}	Normalized beam angular spread, y	0.86
σ_{vg}	Phase velocity spread due to energy spread	3.5
σ_z	Normalized pulse length	1.3
a_0	Normalized initial optical field amplitude	4.0
σ_a	Normalized initial optical pulse length	2.6
z_0	Normalized Rayleigh length	0.26
w_0	Normalized mode waist radius	0.51
ω_β	Betatron oscillation frequency	7.1

Table 18. Dimensionless parameters of the third simulated FEL device.

For the first simulation, it was necessary to update the dimensionless input file each time the number of periods was changed. The number of periods was varied from N=100 through N=200 in intervals of 10, obtaining the highest extraction of η=3.15% at N=130. Figure 35 shows a graph of the extraction versus the number of periods of the undulator. We also considered rotating the undulator 90° by switching the x and y components of the normalized beam radius and angular spread. This change did not make any significant difference in the results.

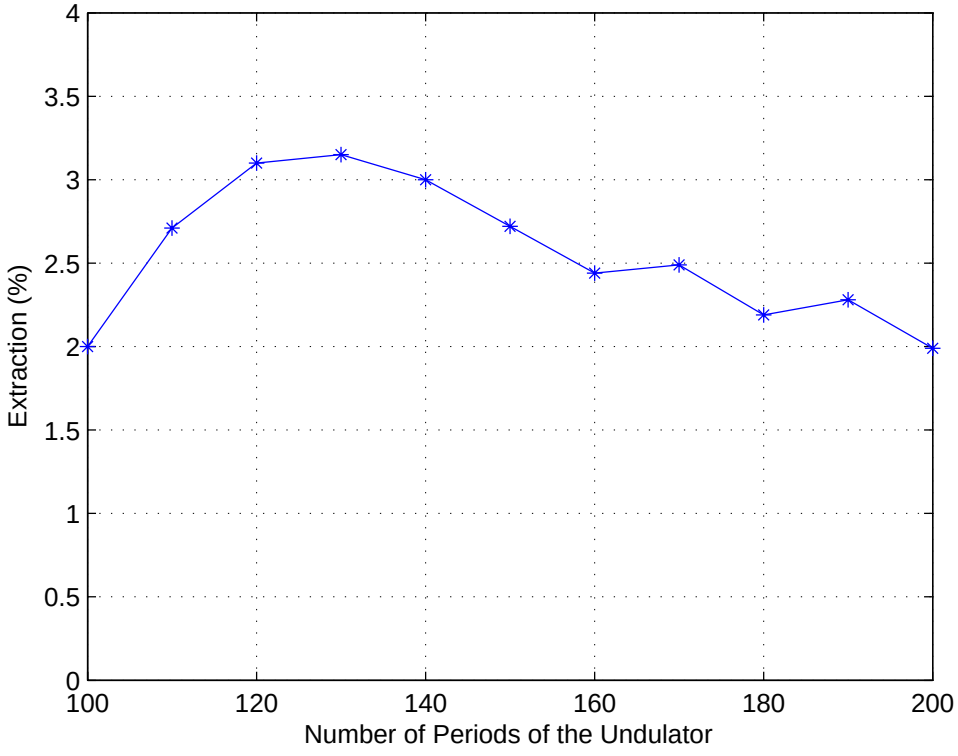

Figure 35. Extraction vs. number of periods of the third FEL.

Figure 38 shows the simulation results for this set of parameters with N=130, which is the optimal value. We can see the power P(τ) growing to saturation at the end of the undulator (τ=1) with an intermediate synchrotron oscillation, and about half of the electrons bunched in phase space (ζ,ν) as shown on phase space diagram.

Using the optimum undulator (N=130), the taper start time was simulated for several values from 0.2 to 0.8 at intervals of 0.1 using a taper rate of 80π. The optimal start time (greatest extraction) was at 0.5 with an extraction η = 3.14%. Figure 36 shows a graph of the extractions versus the taper start times.

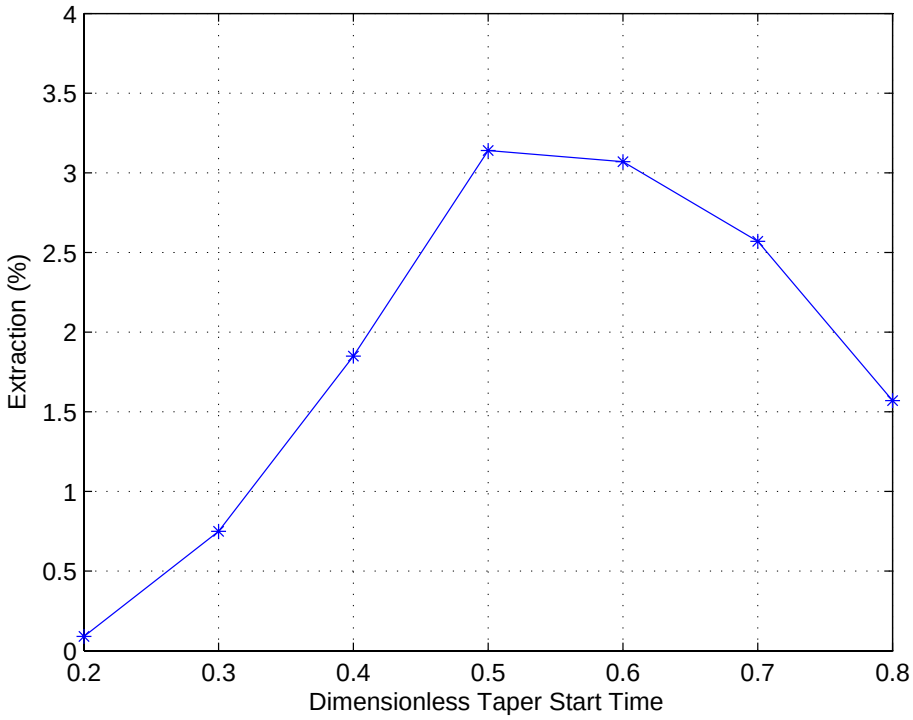

Figure 36. Extraction vs. dimensionless taper start time of the third FEL.

The results for the optimal taper start time (0.5) are shown in Figure 38.

Again, once the optimal value of the taper start time (0.5) was found, it was used to run a set of simulations varying the dimensionless linear taper rate (δ). Simulations were run for δ values from 20π to 110π at intervals of 10π. The most efficient rates were at δ = 80π and δ = 90π with an extraction η = 3.14%. Figure 37 shows a graph of the obtained extractions versus the taper rates. Beyond the peak it is roughly flat.

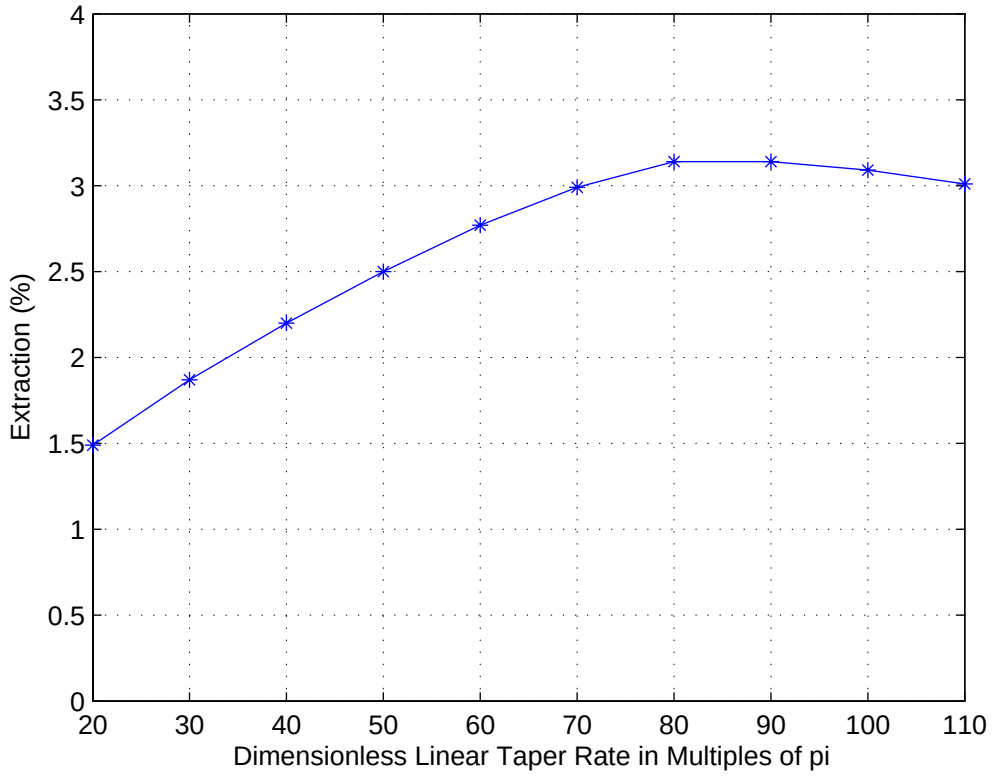

Figure 37. Extraction vs. dimensionless taper rates of the third FEL.

The results for the taper rate δ = 80π are shown in Figure 38.

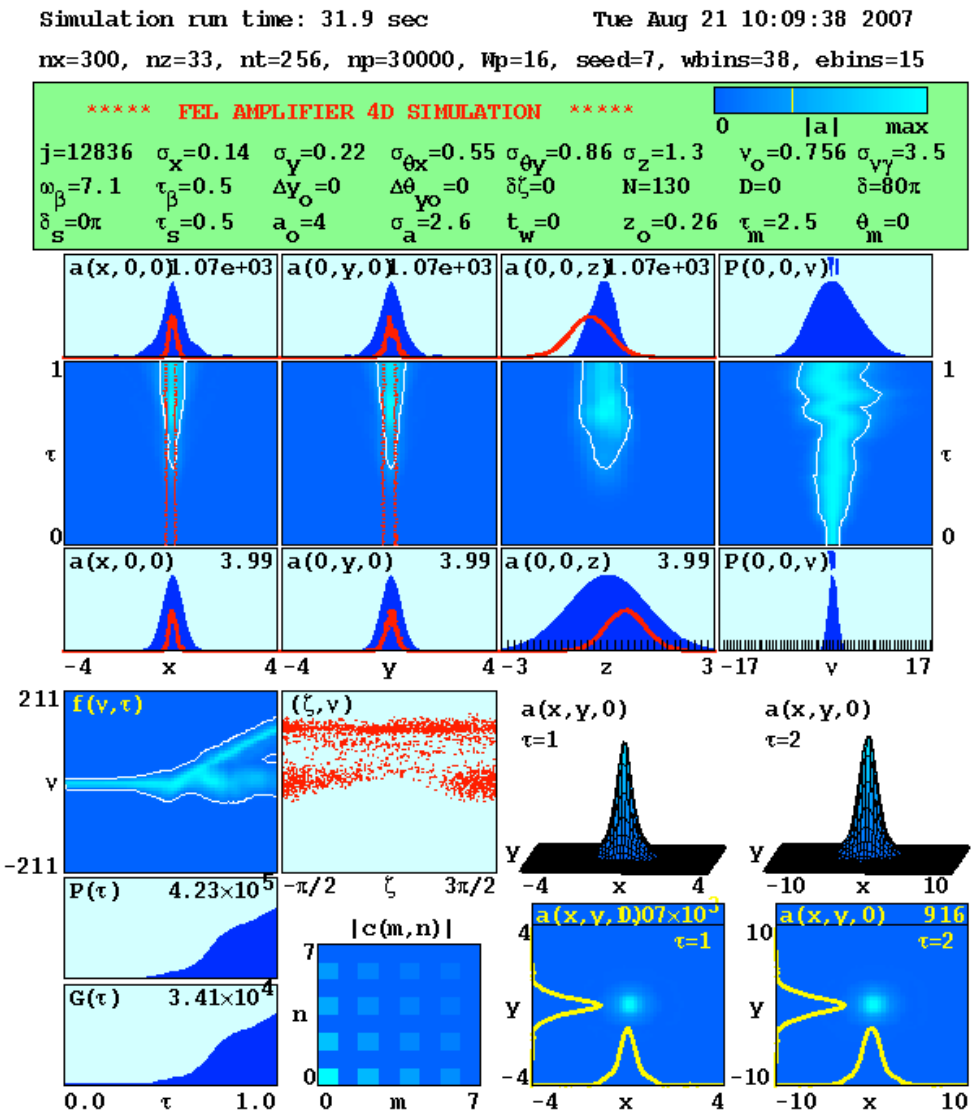

F=0.47, G=3.41e+04, η=0.0314, Δγ/γ=0.131

THEORY: G(jF>>1)=6.73e+04

THEORY: η(jF>>1)=0.0385

a_s=499 at τ_s=0.50, THEORY: a_s=420 at τ_s=0.46

M^2=0.1, $c^2(0,0)$=0.4, $c^2(0,2)$=0.14, $c^2(2,0)$=0.12

Figure 38. Results for N=130 of the third FEL.

THIS PAGE INTENTIONALLY LEFT BLANK

V. CONCLUSION

In this thesis, we have discussed the components and basic theory of a Free Electron Laser (FEL) in order to describe its behavior.

We have explored, by means of simulations, three designs of Free Electron Lasers in the amplifier configuration, using different parameters to establish a desired power output and optical wavelength. It has been shown that undulator taper has an important effect increasing the single pass extraction.

For the low power (~100kW) FEL examples, extraction between 1% and 2% was found. Even after optimizing the taper parameters, the extraction did not improve much. We tried to obtain higher extraction by changing electron beam parameters, such as pulse duration, bunch charge, and emittance, but found no significant improvement. We conclude that these three parameters did not have a large effect on the final extraction of the system.

In higher power (~3MW) FEL examples, it was found to be easier to obtain higher extraction. For high power FEL examples, we have obtained extractions above 3%, compared to 1% or 2% in low power devices.

Future investigation should focus on taper parameters and undulator characteristics, as an important way to improve FEL designs.

THIS PAGE INTENTIONALLY LEFT BLANK

LIST OF REFERENCES

[1] "Laser." Wikipedia, the free encyclopedia, *[http://en.wikipedia.org/wiki/Laser]* 04 April 2007.

[2] Welcome to IEEE Xplore 2.0 The history of the free electron laser. *[http://ieeexplore.ieee.org/xpls/abs_all.jsp?tp=&arnumber=110735]* 4 April 2007.

[3] William B. Colson, Class Notes, ***PH 4858 - Electric Ship Weapon Systems***, Fall 2006.

[4] George R. Neil, "***DEPS Short Course on FELs 2002 - Practical Implementation of FELs",*** 12 November 2002.

[5] Dinh C. Nguyen, "***DEPS Short Course on FELs 2002 - FEL Amplifiers"***, 12 November 2002.

[6] "Free electron laser." Wikipedia, the free encyclopedia, *[http://en.wikipedia.org/wiki/Free_electron_laser]* 04 April 2007.

[7] Colson W.B., C. Pellegrini and A. Renieri,eds. ***Free Electron Laser Handbook***. The Netherlands: Elsevier Science Publishing Co. Inc. 1990.

[8] G. Travish, N. Arnold and R. Koldenhoven, "The Drive Laser for the APS LEUTL FEL Rf Photoinjector". [***http://www.myaxys.com/travish/publications/FEL99_TUP39.pdf***] 15 August 2007.

THIS PAGE INTENTIONALLY LEFT BLANK

INITIAL DISTRIBUTION LIST

1. Defense Technical Information Center
   Ft. Belvoir, Virginia

2. Dudley Knox Library
   Naval Postgraduate School
   Monterey, California

3. Professor William B. Colson
   Naval Postgraduate School
   Monterey, California

4. Professor Joseph Blau
   Naval Postgraduate School
   Monterey, California

5. Chairman, Physics Department
   Naval Postgraduate School
   Monterey, California

6. Professor Robert Armstead
   Naval Postgraduate School
   Monterey, California

7. Professor Peter Crooker
   Naval Postgraduate School
   Monterey, California